National Technical University of Athens

School of Civil Engineering

Department of Water Resources and Environmental Engineering

Diploma Thesis

Modeling shelter abundance for juvenile Atlantic salmon using SSIIM 2

Case study, HPP residual flow reach in Turgi, Switzerland

Author: Spyros Pritsis

Supervisors: Prof. Anastasios Stamou

Department of Water Resources and Environmental Engineering, NTUA

Prof. Nils Rüther

Department of Civil and Environmental Engineering, NTNU

Athens, March 2021

Acknowledgements

I would like to thank Professor Nils Rüther, Research Adviser Kordula Schwarzwälder and the researchers and fellow students at the department of Civil and Environmental Engineering at NTNU for the invaluable help and support they provided me.

I would also like to thank Professor Anastasios Stamou and the researchers of the Laboratory of Applied Hydraulics for their help during the time it took me to complete this thesis and more importantly for their contribution in my understanding and subsequent enamourment of numerical modeling without which I would not have chosen to carry out this thesis.

Table of Contents

List of Figures

List of Tables

Abstract

Nowadays, the aquatic biodiversity is highly under pressure due to anthropogenic changes of the rivers such hydraulic structures changing the diversity of flow and aquatic fauna as well as sediment continuity. This can have severe consequences on the fish population in the river reach. Fish are strongly depending on a certain substrate composition throughout all their life stages. Juveniles for example are depending on a certain availability of shelter in the substrate in order to survive this stage.

Therefore, we investigate the effects of changes in the sediment composition at a hydropower plant in Switzerland on the availability of potential shelter for juvenile fish. By utilizing the observed correlation between parameters describing the fine tail of a riverbed's grain size distribution and shelter abundance for juvenile Atlantic salmon, we predict the available shelter in a river reach by using a 3D hydrodynamic numerical model directly coupled to a morphodynamic model. The initial substrate composition was assumed to be spatially uniform, its parameters based on a grain size distribution curve derived from collected sediment samples.

This model can now be used for habitat improvement scenario modeling. Based on the assumption that a specific mixture of sediment coming from upstream travelling through the river reach, will positively influence the potential shelter availability, different scenarios can be investigated. The baseline discharge was set to 100 m^3 /s and was applied for 24 hours. The resulting bed and sediment distribution changes create a map of the potential shelter availability of this grain size mixture. Then, two scenarios with sediment inflow from the upstream boundary were simulated. One coarse and one fine mixture of sediment were chosen as inputs, with the goal of investigating their impact on shelter abundance. The former designed to have a positive effect while the latter expected to reduce interstitial voids in the substrate and have a negative effect on available shelter.

1 Introduction

1.1 Motivation

With renewable energy accounting for more than 18% of energy consumed in the EU (Eurostat 2020) with the target of reaching 32% by 2030 (International Renewable Energy Agency 2020) and hydropower plants alone providing up to 28% in some EU countries (Portuguese Renewable Energy Association 2020), understanding and mitigating any negative environmental impacts these power plants have is a necessity. Hydropower plants regulate water and sediment flow both upstream and downstream of their position, that can drastically impact the area's ecosystem. Those changes can negatively influence the shelter abundance for fish in the area, one of the phenomena that plays a major role in shelter reduction is embeddedness (Sylte and Fischenich 2003). The availability of habitats with abundant shelter is one of the key factors for stabilizing fish populations in HPP affected rivers (Schwarzwalder et al. 2018).

As computing power becomes more affordable and algorithms used in CFD models progress, the use of these models for simulating water flow in river reaches and sediment movement at their beds has become widespread. In the context of research, with the goal of developing better models to simulate real phenomena with as much accuracy as possible; and in numerous practical applications, from predicting flood fields to designing fish-passes.

Even though there is an understanding that substrate size in rivers can be a limiting factor for shelter availability for fish, which in turn plays a role in habitat quality (Heggenes et al. 1999; Finstad et al. 2007; Morantz et al. 1987), most models don't take into consideration the key parameters that are shown to be correlated with shelter availability —e.g. the D_5 percentile of the sediment (Jocham 2010)— when calculating the habitat quality. By adding these variables to the process of determining habitat quality for juvenile Atlantic salmon the model's output should be better corresponding to the real conditions of the habitat at the area of study.

In his MSc thesis Jocham (2010) aimed to develop a correlation between shelter abundance for juvenile Atlantic salmon and substrate parameters, mainly grain size distribution. Even though the samples analyzed by are not enough to give a certain answer, a correlation

between the D_5 percentile of the grain sizes and shelter abundance is witnessed. It is also proposed that the D95 percentile is used as a limiting factor for the existence of shelter. Meaning that if the coarsest 5% of the sample does not pass a certain size threshold, the salmonids will not be able to find shelter no matter what the D_5 percentile indicates.

The goal of this thesis is to utilize the correlation witnessed between shelter availability for juvenile Atlantic salmon and grain size distribution by Jocham (2010) in the framework of habitat modeling. By developing a numerical model simulating water flow and sediment movements in a segment of the Limmat river in Switzerland the changing of the bed conditions can be predicted and then translated to shelter availability which is a determining factor for habitat quality. Introduction of different sediment mixtures is also considered as a means of increasing the D_5 percentile of the river bed, resulting in more abundant shelter.

As a part of the FIThydro (Fish friendly Innovative Technologies for hyrdropower) broader project this thesis has aims to contribute to the realization of some of the objectives set in the project's proposal. The main FIThydro objectives pertinent to this thesis' goals are:

- Assessing the response and resilience of fish populations in HPP affected rivers
- Developing innovative methods and models for undertaking environmental assessment of HPPs on rivers

1.2 Basic concepts

To study and develop methods to improve the habitat conditions for Atlantic Salmons in river reaches an understanding of their general behavior and more importantly their behavior during spawning season and through their juvenile stage is essential. Furthermore, identifying spawning bottlenecks connected to habitat and flow conditions and gaining insight into the mechanisms causing them is necessary. In the chapters below a quick overview of the existing literature on those subjects is given.

1.2.1 Atlantic Salmon and its habitat

The Atlantic salmon is an anadromous fish, this means it spends its life at sea and migrates to fresh water to spawn. The spawning usually happens in autumn in the upstream parts of rivers (Armstrong et al. 1998). The spawning procedure starts with the females finding a place with

suitable habitat conditions and digging a pit with their tails where they will lay their eggs (Esteve 2005). When the pit is dug the female signals the male and after fertilizing the deposited eggs the nest is closed. After 45-140 days alevins hatch and stay hidden in their yolk sac for 4 to 5 weeks. After this period, they emerge from the gravel as fry until they reach a length of 5 to 8 cm. Then the fish remain in fresh water for 2 to 4 years, at this stage it's called a parr. After this the fish reach a length of 12 to 24 cm and are now ready to migrate downstream to the sea, this is called the smolt phase. After spending one year or more at sea, the fish migrate up their home river and spawn. Usually they die after spawning due to exhaustion (Mills 1989).

It has been recognized that juvenile Atlantic salmon behavior patterns differ from summer to winter. Studies have shown that when the temperature drops below 10°C salmonids change their behavior from feeding and being active during the day to seeking shelter in crevices and under stones in daytime and feeding in nighttime (Armstrong et al. 2003; Valdimarsson and Metcalfe 1998; Fraser et al. 1993). A hypothesis as to why that change happens is to remain unseen from predators that hunt in daytime (Armstrong et al. 2003). This means that shelter availability and substrate quality is an important factor for juvenile salmonids survival, especially during the winter where it becomes a dominant microhabitat characteristic (Heggenes et al. 1999).

Habitat can be described as the sum of all the physical and chemical variables that affect an animal. Both the spatial and temporal scales of what the limit of an animals' habitat is can vary. For the Atlantic salmon, in the spatial domain, scales may range from fractions of the reach to global and in the temporal domain, from fractions of a second to geological time (Armstrong et al. 2003).

The habitat features that are most important to salmonid populations are depth, current, substrate and cover (Armstrong et al. 2003; Kondolf and Wolman 1993). Preferred values for these parameters according to literature are shown in Table 1.1

Table 1.1 Reported rearing habitat used by Atlantic Salmon (Armstrong et al. 2003)

Habitat variable	Measure	Values	Authors
Snout water velocity	Range	5-35 cm	(Morantz et al. 1987)
	Range	0-20 cm	(Heggenes et al. 1999)
	Range	10-50 cm	(Rimmer et al. 1984)
Mean column velocity	Maximum	>60 cm	(Heggenes et al. 1999)
	Maximum	<120 cm	(Morantz et al. 1987)
	Minimum	<20 cm	(Heggenes et al. 1999)
	Utilized preference	50-65 cm	(Symons and Heland 1978)
	Utilized preference	10-65 cm	(Heggenes 1990)
Water depth	Range	20-70	(Symons and Heland 1978; Rimmer et al. 1984; Heggenes 1990; Morantz et al. 1987)
	Range	64-512+ cm	(Heggenes 1990)
Substrate size	Range	<20 cm	(Heggenes 1990; Heggenes et al. 1999; Symons and Heland 1978)

The values of most of these parameters vary considerably, Armstrong et al. 2003 gives some potential explanations for that. One is that fish can genetically adapt to their local habitats, for example their morphology can change to suit their habitat. Another explanation might be salmon's tolerance for a wide range of conditions. Furthermore, different studies examine river reaches with different ecologies but this is not taken into account when comparing their results. This means the models trying to establish a connection between habitat characteristics and habitat quality by assuming habitat quality is directly analogous to fish population may give incorrect results. One reason for this is that at densely populated rivers fish will also use sub-optimal habitat due to high competition for the limited spawning grounds creating scarcity of better choices. Lastly, considering the habitat variables independently of each other is an oversimplification. In reality the fish respond a combination of variables. For example, brown trout chose positions by finding the best combinations of water depth and velocity and not by considering each variable independently (Shirvell and Dungey 1983; Hedger et al. 2005).

1.2.2 Embeddedness

Embeddedness is a term describing the degree to which gravel sized and larger particles of the substratum are surrounded or covered by fine sediment (Fitzpatrick et al. 1998). Embeddedness reduces interstitial space and permeability in the substratum, negatively affecting shelter abundance for Atlantic salmon (Finstad et al. 2007; Scheurer et al. 2009; Sylte and Fischenich 2003).

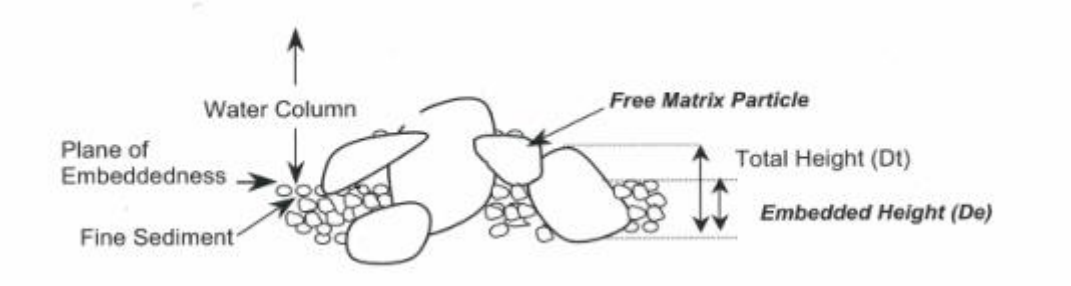

Figure 1.1 Embeddedness Illustration (Sylte and Fischenich 2003)

A visual representation of varying degrees of embeddedness is shown in Figure 1.2. Starting from no embeddedness, far left, to a very high degree of embeddedness, far right.

Figure 1.2 Degrees of embeddedness (Eastman 2004)

It is obvious that the higher the degree of embeddedness of the substrate, less interstitial space is clear of fine sediment meaning that the crevices juvenile Atlantic salmon use for shelter are reduced. The degree of embeddedness is affected by various substrate and water flow parameters, focusing on the grain size distribution as a determining factor we can surmise that the more dominant the fine sediment size tail of the curve, the higher the degree of embeddedness.

Based on that and on previous studies showing that embeddedness plays a major role in habitat quality and abundance (Sylte and Fischenich 2003) Jocham (2010) and Szabo-Meszaros (2015) studied the relationship between the biological measure of shelter abundance for juvenile salmonids and the physical measures of grain size distribution in various rivers in Norway (Lundesokna, Gaula and Nidelva) and found a strong correlation between the characteristics of the sediment grain size curve, especially the fine tail of the curve, and the available shelter for the fish.

2 Materials and Methods

2.1 Study site

The river segment modeled in this thesis is situated directly upstream of the Schiffmühle hydro power plant in Switzerland on river Limmat. It is a residual flow reach with a minimum discharge of 9 m^3/s. There are three inflows, a fish-pass (A) that has a steady discharge of 0.67 m^3/s, a weir (B) that regulates the waterflow into the reach and a side-weir (C) that serves as an overflow from the main channel that leads to the hydro power plant. A satellite photograph of the study site can be seen in Figure 2.1. The flow direction is from right to left (west to east). This direction is kept in all the simulations, unlike usual conventions all figures of the modeled river segment should be seen from right to left.

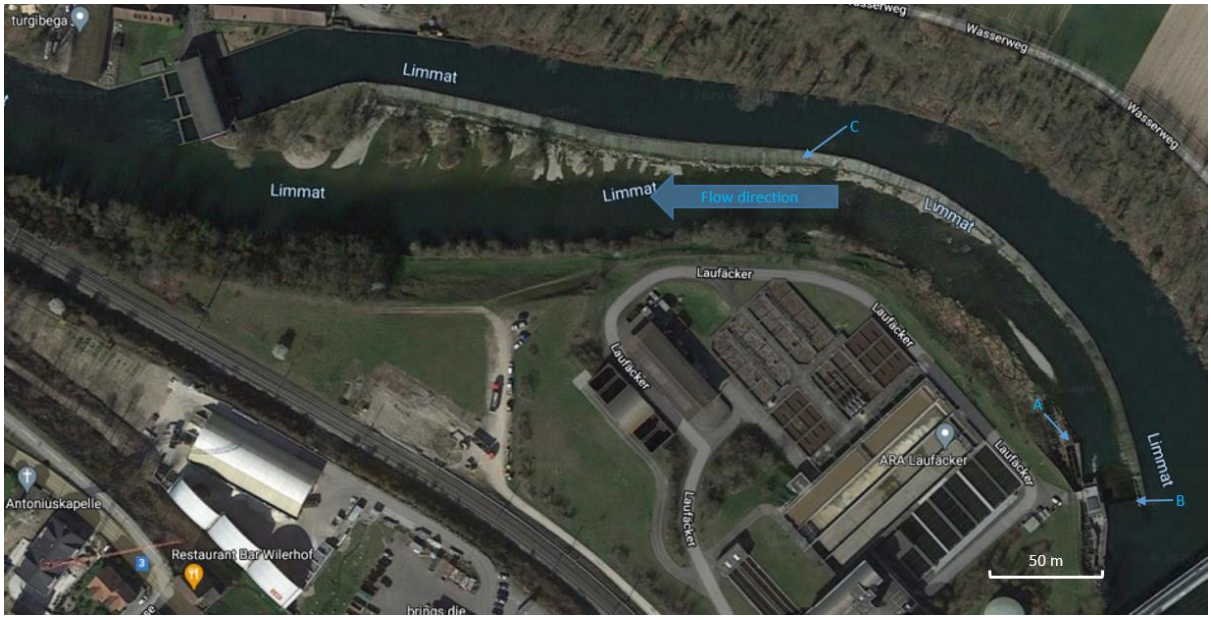

Figure 2.1 Limmat river segment (Google maps)

Typical for a HPP residual flow reach the study site has a regulated inflow with flash flood like events— weir opening. The reach bed mainly comprises of gravel and cobble, with a median bed material particle size of 60.4 mm. The average slope is 1% resulting in relatively low velocities, expected from valley rivers.

2.2 Measurements

The data used for setting up the simulations was acquired by field measurements from the reach of interest, downstream from the Schiffmühle fish-pass. Discharge data was collected by measuring water flow at critical points along the stream. The geometrical data is cross-sectional. Sediment grain size distribution and other riverbed parameters were acquired by following the procedure used by existing literature on the subject of linking shelter availability with substrate conditions (Finstad et al. 2007; Jocham 2010).

A 50x50 cm square frame was tossed in 16 locations of shallow water along the riverbed and on the river banks, before starting collecting the samples, the locations were photographed. Shelter abundance was measured using 3 PVC tubes with diameters of 5, 8 and 13 mm. For each tube, voids that it fit in and were deeper that 3 cm were counted. The voids were divided in three categories depth-wise, >3 cm, >7 cm and >12 cm. The tube diameter giving results with the strongest correlation to the growth of the fish is 13mm (Jocham 2010). Then a pebble count was done by diagonally attaching a string on the square and measuring the diameter of all the stones directly below the string. After all the parameters that require an undisturbed sample were measured, the surface layer was collected and sent for sieving at a laboratory in ETH. Ten sediment samples from different areas of the river and its banks were analyzed and a grain size distribution curve was plotted for each of them.

2.3 CFD software

A mathematical model is a mathematical representation of an actual situation that has the ability of qualitative or quantitative predictions (Kondolf and Piégay 2003; Winston 2004). A wide range of mathematical models are used for solving a plethora of engineering problems. These models can be deterministic or stochastic, in the case of hydrodynamic and morphodynamic modeling deterministic models are preferred. This means that numerical algorithms are utilized to solve (or approximate) a set of equations governing the physical properties of the simulated materials. Advances in computer science and mathematics provide us with better algorithms, while advances in physics and engineering provide us with more insight in the workings of fundamental physical processes allowing us to better describe them with accurate equations.

2.3.1 Equations

In the current thesis SSIIM 2, a 3D CFD software was used to model water flow sediment movement. SSIIM solves the Reynolds averaged Navier-Stokes equations for turbulent flow in a three-dimensional geometry ((2.1), (2.2)), discretized with the finite volume method, to obtain the water velocity and pressure.

$$\nabla \rho u = 0 \tag{2.1}$$

$$\rho\left(\frac{du_i}{dt}\right) = \rho g - \frac{\partial p}{\partial x_i} + \frac{\partial}{\partial x_j}\tau_{ij} \tag{2.2}$$

Written in tensor form, where τ_{ij} is the total shear stress that using the Boussinesq (1877) approximation can be described as:

$$\tau_{ij} = \mu\frac{\partial u_i}{\partial x_j} + \rho\left[\nu_T\left(\frac{\partial u_i}{\partial x_j} + \frac{\partial u_j}{\partial x_i}\right)\right] \tag{2.3}$$

To calculate the turbulent shear stress (Reynolds stress), the standard k-ε model is used (Launder and Spalding 1974). The SIMPLE algorithm is used for pressure correction. A second-order upwind scheme is used for the convective terms of the velocity equations and a first order power law scheme for the k-ε turbulence equations. For the cells near the river bed, rough wall laws (2.4) are applied (Olsen 2018).

$$\frac{U}{U_*} = \frac{1}{\kappa}\ln\left(\frac{30y}{k_s}\right) \tag{2.4}$$

$$U_* = \sqrt{\frac{\tau}{\rho}} \tag{2.5}$$

Where U is the velocity in the cell near the wall, U_* is the shear velocity (2.5), κ is an empirical constant equal to 0.4, y is the distance from the wall to the center of the cell and k_s is the roughness. Water density, ρ, is set to 1000 kg/m^3 and τ is the bed shear stress.

Simulations were done with 2 different timesteps for each scenario, 10 and 20 seconds. With a maximum velocity of less than 3 m/s and cell length of approximately 1 m, the courant number, calculated using equation (2.6), is not bigger than 25 for the 10 second timestep and 50 for the 20 second timestep in any of the grid's cells.

$$c = \frac{u\Delta t}{\Delta x} \tag{2.6}$$

A variable number of inner iterations was used. This means that an upper limit of 250 inner iterations was set but if the highest residual falls below 10^{-4}, the inner iterations are stopped and a new time step starts.

For the purpose of this thesis, scenarios with and without sediment introduction from the upstream boundary were simulated. For the cases with sediment inflow, algorithms were used for computing both suspended sediment movement and bedload sediment transport. For the cases with no sediment inflow only the bedload transport was calculated.

For the suspended load, the inflow concentration is specified and then SSIIM 2 solves the convection-diffusion equation for the sediment concentration (2.9) in all cells.

$$\frac{\partial c}{\partial t} + U_j \frac{\partial c}{\partial x_j} + w \frac{\partial c}{\partial x_k} = \frac{\partial}{\partial x_j}\left(\Gamma \frac{\partial c}{\partial x_j}\right) + S \tag{2.7}$$

Where c is the suspended sediment concentration. The fall velocity is denoted w. The value of the diffusion coefficient, Γ, is derived by the eddy-viscosity using (2.8).

$$\Gamma = \frac{v_\tau}{S_c} \tag{2.8}$$

Where S_c is Schmidt's coefficient, a correction factor to correlate turbulent diffusivity (governed by Γ) and the eddy-viscosity, v_τ, calculated by the k-ε model.

The last term of the equation, S, is a source term equal to the pick-up rate of sediments from the river bed.

The bedload sediment transport calculation is a two-step process, first SSIIM 2 determines whether or not each sediment size has the capacity to move under the stresses calculated on the river bed and then the volume of the bedload transport is calculated for the sediments that pass the criteria for incipient motion. To do this, first it compares the effective bed-shear velocity calculated at each of the bed cells with the critical bed-shear velocity for each sediment fraction.

To calculate the critical shear stress, τ_c, for incipient motion the Shields parameter equation (2.9) is solved (Shields 1936).

$$\tau_* = \frac{\tau_c}{(\rho_s - \rho) \cdot g \cdot d_i} \tag{2.9}$$

Where τ_* is Shields parameter, set at SSIIM's default value of 0.047. The density of the sediments, ρ_s, is set at 2650 kg/m^3, the water density , ρ, is set at 1000 kg/m^3 and d_i is the grain diameter for each sediment fraction in mm.

The critical shear stress is transformed to bed-shear velocity using equation (2.5) and then used to calculate the dimensionless transport stage parameter, T, in equation (2.10).

$$T = \frac{(u_*')^2 - \left(u_{*,cr}\right)^2}{\left(u_{*,cr}\right)^2} \tag{2.10}$$

Where $u_{*,cr}$ is the critical bed-shear velocity and u_*' is the effective bed-shear velocity related to grains. The effective bed-shear velocity is used instead of the calculated bed-shear velocity to eliminate the effects of bedform roughness on the bed-shear velocity since it does not contribute to bed-load transport. This is done by calculating the effective bed-shear velocity using the cross-sectional depth averaged velocity, $\bar{u}$, and the Chézy coefficient, C', as seen in equation

$$u'_* = \frac{\bar{u}\sqrt{g}}{C'} \tag{2.11}$$

$$C' = 18\log\left(\frac{12R_b}{k_s}\right) \tag{2.12}$$

To calculate the Chézy coefficient the hydraulic radius related to the bed, R_b, and the grain roughness on the bed, k_s, is used.

If the effective bed shear velocity surpasses the critical value, meaning that the transport stage parameter is a positive number, sediment movement is calculated using the van Rijn (1984) formula for bed-load sediment transport shown in equation .

$$\frac{q_b}{{d_i}^{1.5}\sqrt{(s-1)g}} = 0.053\frac{T^{2.1}}{D_*^{0.3}} \tag{2.13}$$

Where q_b is the bed-load transport in m^2/s, d_i is the particle diameter for each sediment grain size, $s = \rho_s - \rho$ is the specific density, T is the dimensionless transport stage parameter described in equation (2.10) and D_* is the dimensionless particle parameter described in equation . To calculate D_* one more variable input is required, the kinematic viscosity coefficient, v.

$$D_* = d_i\left[\frac{(s-1)g}{\nu^2}\right]^{1/3} \tag{2.14}$$

Bed changes are calculated for each time step, slightly altering the geometry. Subsequently, the grid is altered to fit the updated geometry. The next time step uses the new modified bed levels and grid and the RANS equations are solved on the new grid before the sediment calculations take place again.

2.3.2 Geometry

A 3D computational grid was created, using cross-sectional data measured in March 2018. From this data, the bed levels are interpolated and implemented to the grid. The bed levels

interpolation was done with the cross-section algorithm of SSIIM 1. By using this algorithm, the interpolation routine identifies the cross-sections in the point cloud and linearly interpolates the bed levels between a point and the closest point to it, searching vertical to its cross-section. Then the grid was transferred to SSIIM 2. The grid has 300 and 40 cells in the two horizontal directions. In the vertical direction up to 11 cells are used, depending on the water depth. The total length of the simulated part is 390 m. In Figure 2.2, Figure 2.3 and Figure 2.4 the raw geometrical data, a top down view of the grid and the final interpolated bed levels mapped over the river geometry are shown respectively.

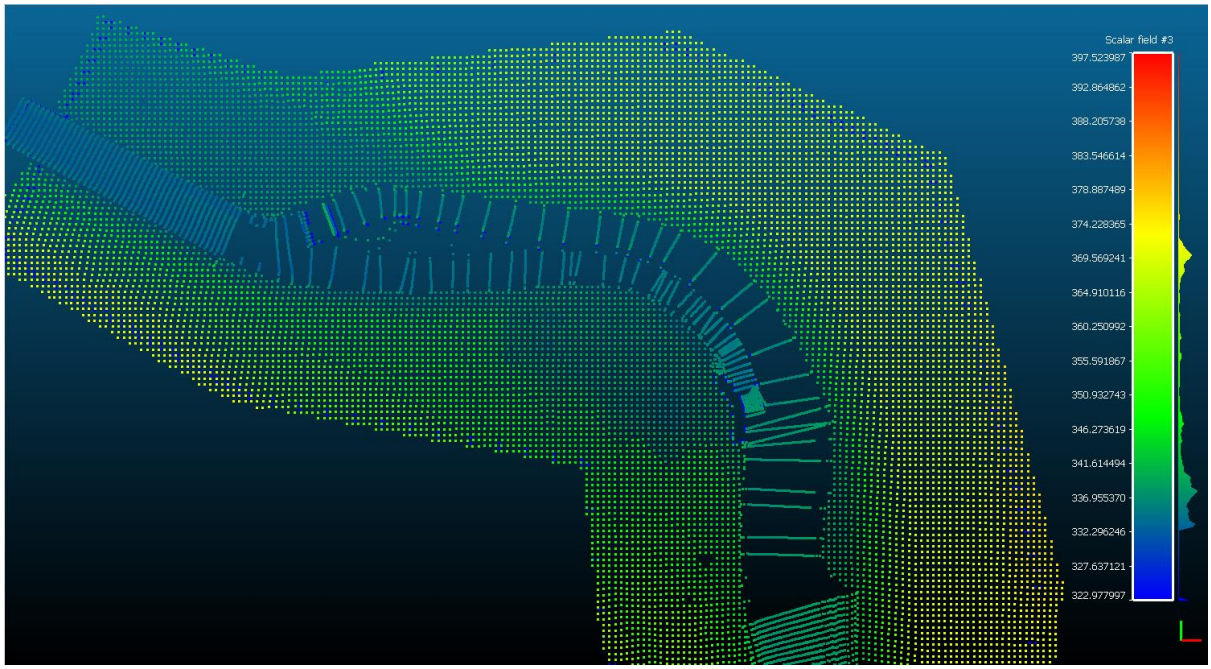

Figure 2.2 Measured bed levels (Point cloud)

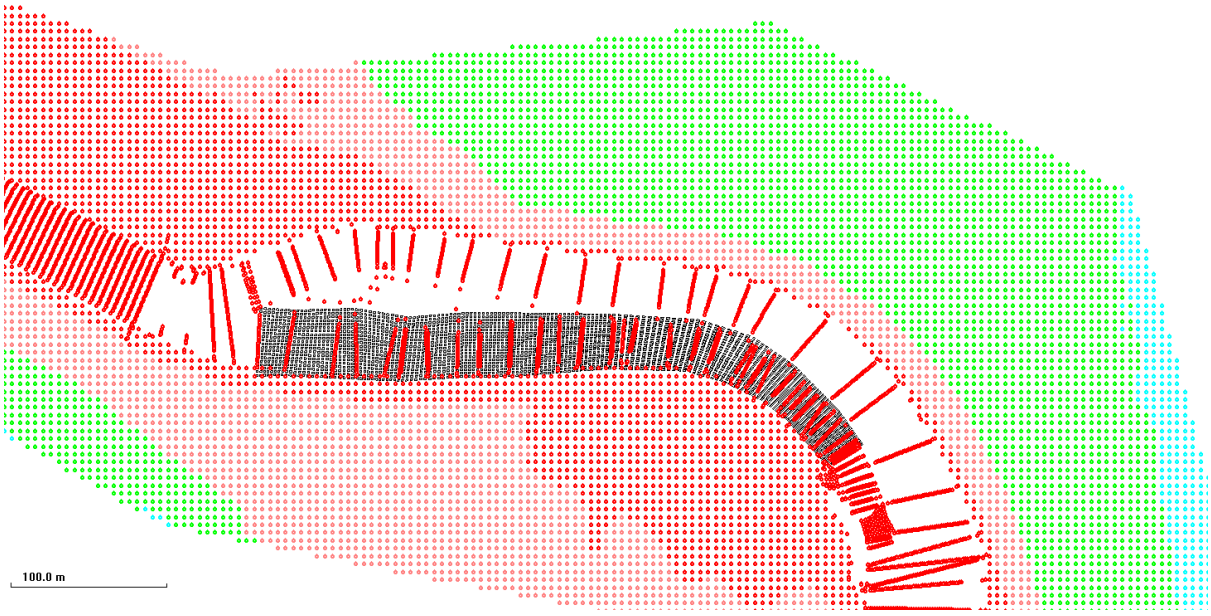

Figure 2.3 Grid created in SSIIM 1

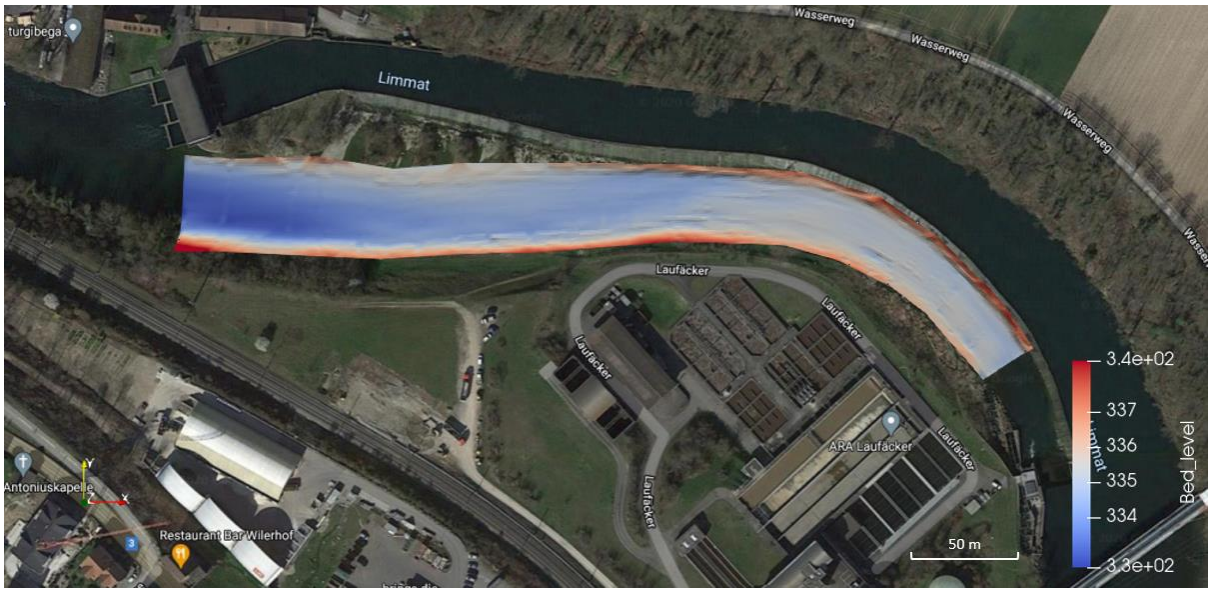

Figure 2.4 Interpolated bed levels (Satellite image taken from Google Maps)

SSIIM 2 divides the riverbed in 2 layers, the active and the inactive layer. Sediment from the active (top) layer can be transported by the flow while the inactive (bottom) layer functions as a non-movable bed. The active layer has a fixed thickness, meaning that at the end of each

time-step sediment is moved to the inactive layer in cells that there has been deposition and the opposite happens in cells where there is erosion.

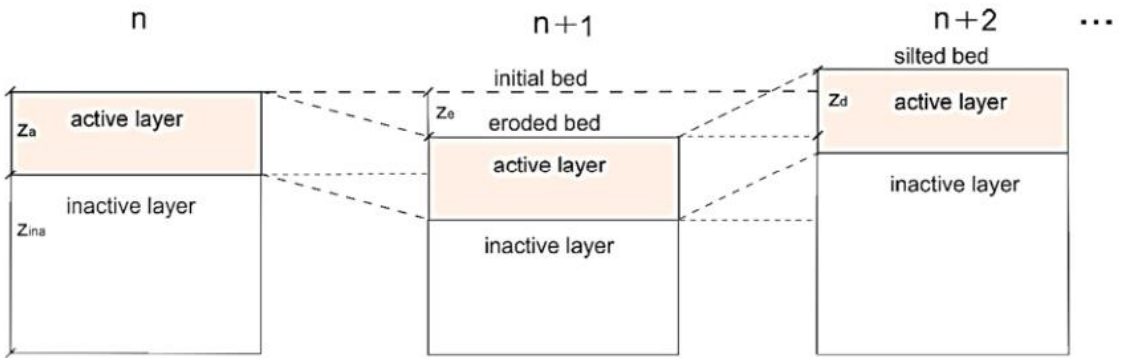

Figure 2.5 Active layer adjustment sketch (Zhang et al. 2015)

The active sediment thickness was set to 0.3 m and the total bed thickness to 10 m.

2.3.3 Initial and boundary conditions

A sloped water surface was defined as the initial water elevation. The water level was set at 335.5 m at the downstream boundary and 337 at the upstream boundary, changing with 0.25 m increments. This gives values for the initial water depth of the reach that range up to 3 m close to the downstream boundary.

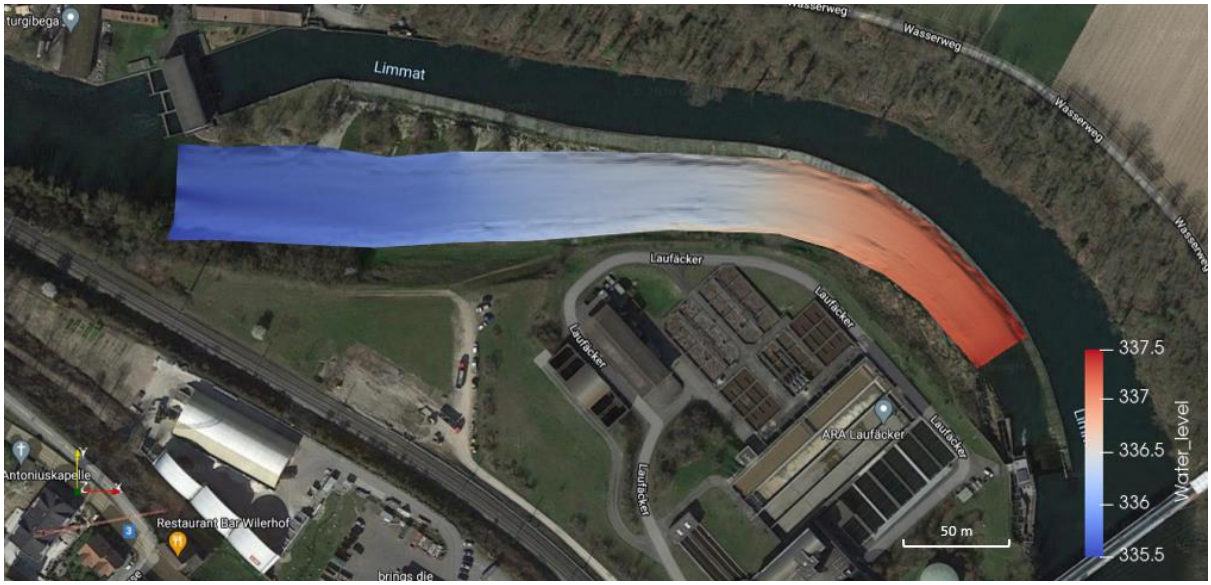

Figure 2.6 Initial water level

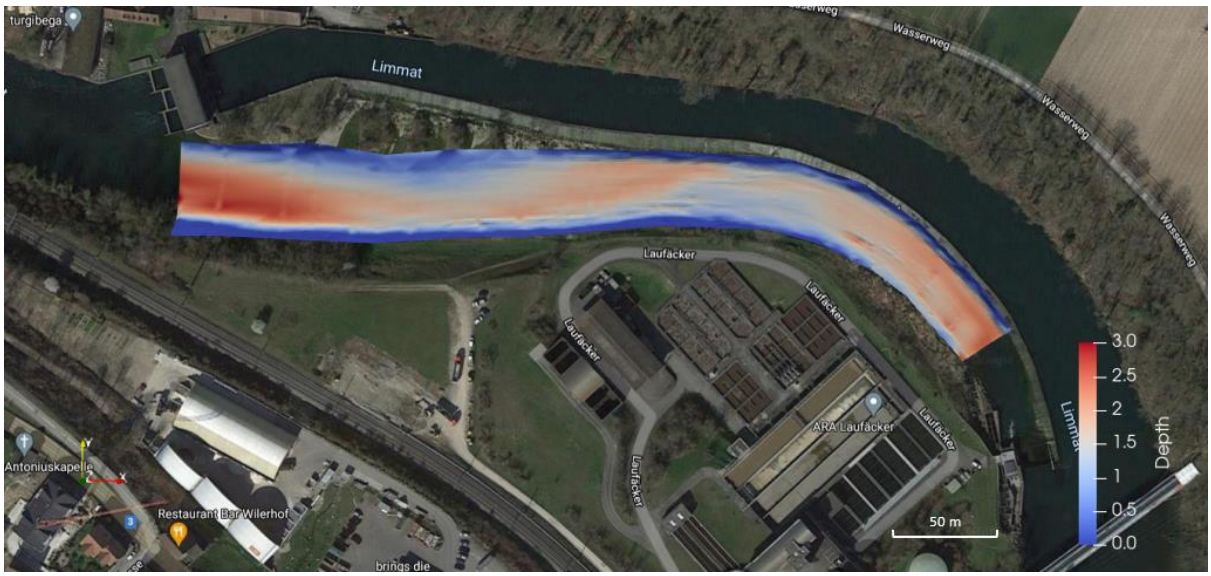

Figure 2.7 Initial water depth

As discharge input data 100 m^3/s was chosen, being a value that is realistic for a high discharge scenario in the residual flow reach of interest and also creating velocities high enough to produce significant bed movements. A simulation with 10 m^3/s discharge was run to compare the results with ADCP measured velocities from the same reach, gathered on 10.01.2018. Velocity profiles from 12 points were compared with the ADCP measurements to calibrate the roughness parameter of the model.

Spillover from the main channel over the weir was neglected, since it is not significant compared to the 100 m^3/s upstream inflow that was chosen for the simulations.

The sediment grain size curve was derived by averaging the curves from a grain size analysis (sieving) of sediment samples from 10 locations on the river bed, gathered —as described in the Measurements chapter— by collecting the top layer of sediment encompassed in 60x60cm squares positioned at every location. From this sediment grain size curve, a spatially homogeneous grain size distribution was assumed for the river bed. Two more sediment grain size curves were artificially created by skewing the original curve towards the fine tail of the

distribution. Characteristic parameters for each curve are shown in Table 2.1 and the residual sediment weight for each sieve size is shown in Appendix A.

Table 2.1 Percentile values for sediment curves

Percentiles (mm)	Curve 1	Curve 2	Curve 3
D_5	15.2	4.2	4.3
D_{10}	17.0	4.5	4.8
D_{50}	44.3	7.1	8.0
D_{90}	99.6	14.9	63.6

By assuming a spatially homogeneous distribution of sediment in the reach once more and using the 2 artificial curves as an initial condition for the grain sizes making up the river bed, we get a total of 3 different substrate compositions. For these 3 scenarios water flow and sediment movement were simulated. The original and both modified sediment grain size curves are shown in the figures below.

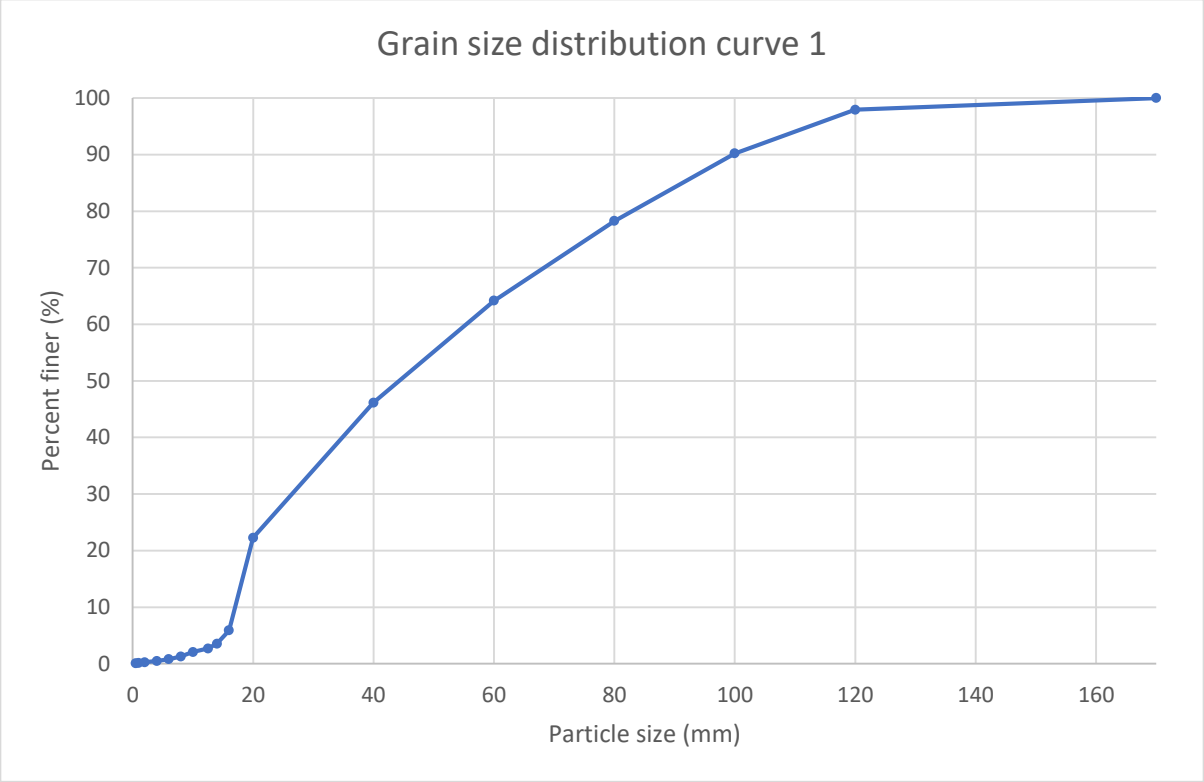

Figure 2.8 Grain size distribution curve 1 (Original measured curve)

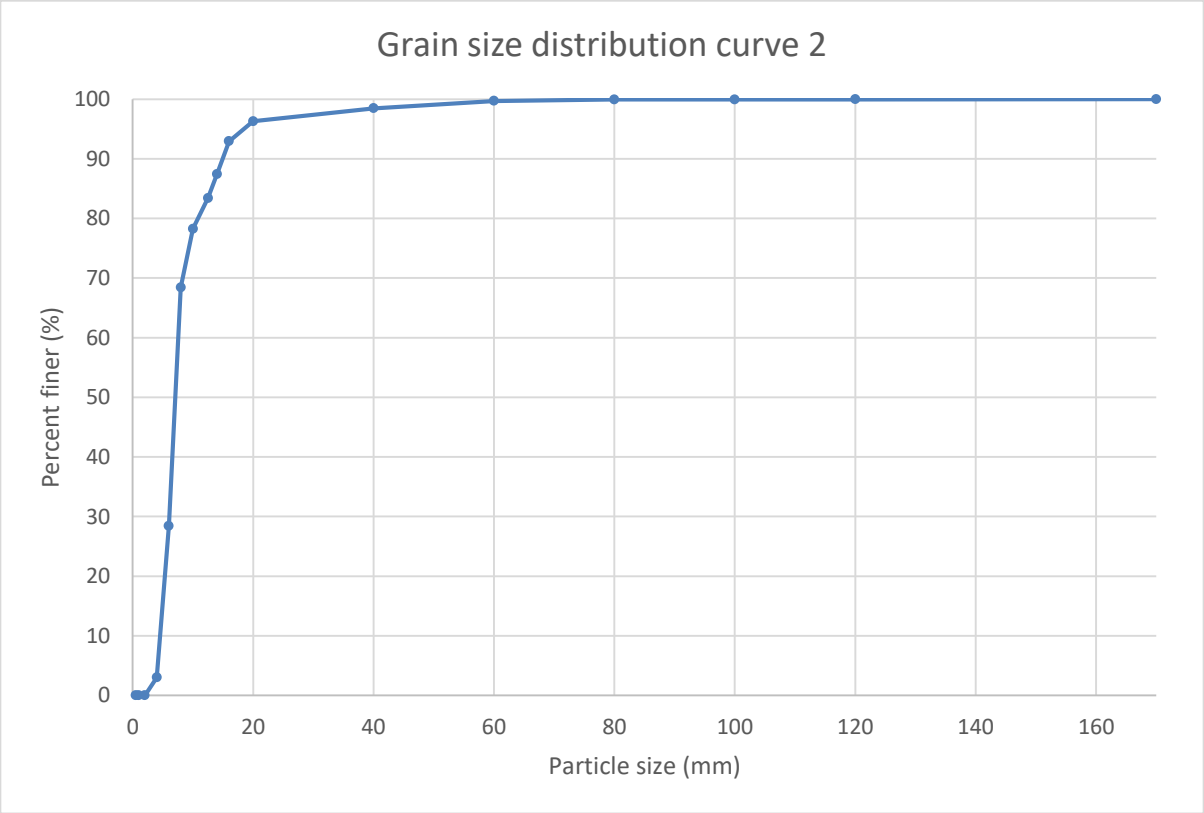

Figure 2.9 Grain size distribution curve 2 (Artificially infused with fine sediment)

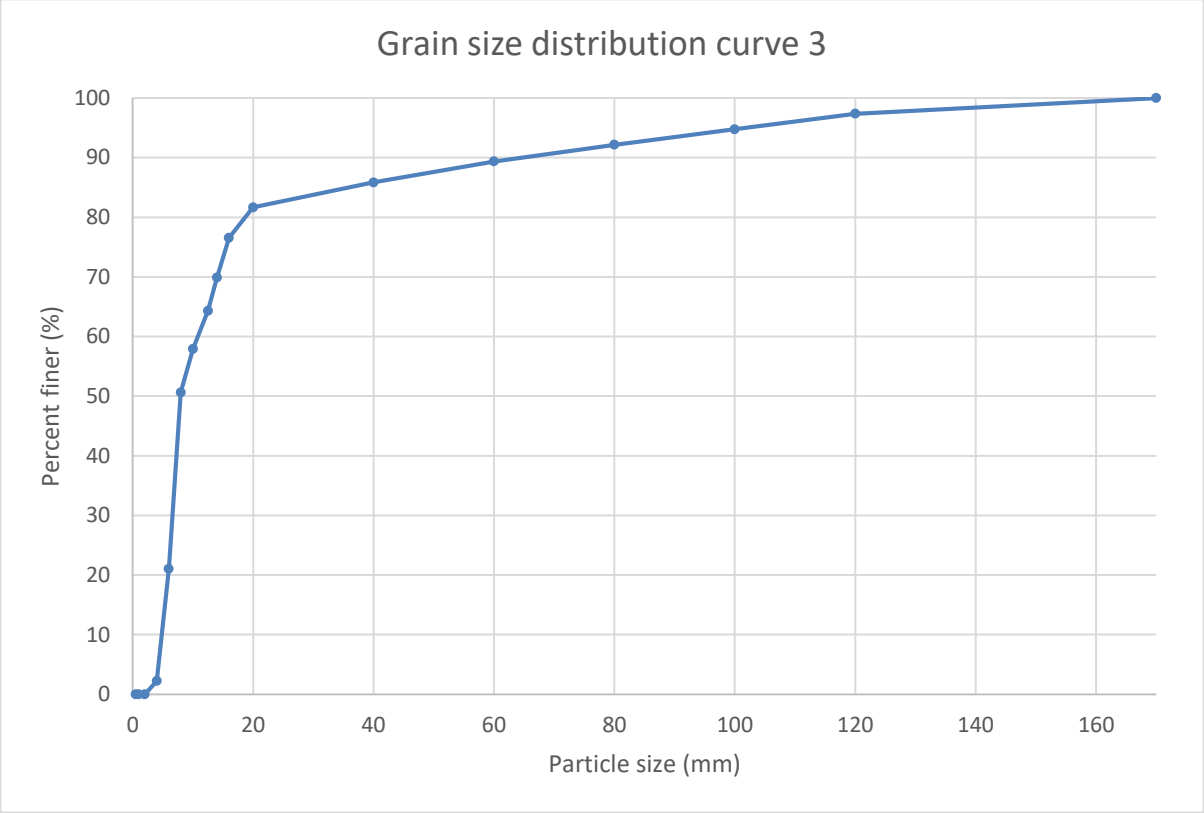

Figure 2.10 Grain size distribution curve 3 (Artificially infused with fine sediment)

Additionally, two cases with sediment concentration at the inflow discharge were simulated. An inflow of a sediment mixture was selected as the boundary condition for each case. Meaning that the water passing through the inflow cross-section is infused with a mixture of sediments whose concentrations were defined for the given grain sizes. The sediment mixture for the first case was selected following guidelines for Atlantic salmon habitat improvement set by Forseth and Harby (2014); meaning that 20% of the grains had diameters between 8 and 16 mm, 60% had diameters between 16 and 32 mm and 20% had diameters between 32 and 64 mm. The sediment mixture for the second case was based on the second grain size distribution curve, meaning 90% of the sediment's grain size is below 15 mm. This very fine mixture is expected to result in reduced interstitial spaces and higher degrees of embeddedness, hence negatively impacting the habitat quality of the substrate.

These cases were simulated with the goal of assessing the consequences on habitat quality in the reach if a favorable, in the case of the first mixture, or an unfavorable, in the case of the

second mixture, grain size distribution is introduced on the upstream boundary and transported downstream by the flow.

The total sediment concentration at the inflow was set at 0.001 kg/m^3 resulting in a sediment inflow of 0.1 kg/sec for the simulated discharge. The resulting concentrations are shown in Table 2.2.

Table 2.2 Sediment inflow concentrations

Grain size (mm)	Concentrations (kg/m^3)	
	Scenario 1	Scenario 2
40	2×10^{-4}	2×10^{-5}
20	6×10^{-4}	3×10^{-5}
16	1×10^{-4}	1×10^{-4}
10	1×10^{-4}	5.5×10^{-4}
4	0	3×10^{-4}

Both of the cases simulating a sediment inflow in the reach were done using the measured sediment grain size distribution (Figure 2.8) as the initial substrate condition for the riverbed.

2.3.4 SSIIM input and output files

All of the input data described in the previous chapter is fed to SSIIM 2 by writing plain text files with specific layouts and names. The only input given to the model via the SSIIM 2 GUI is the grid, which is defined in the Grid Editor tab of the GUI. SSIIM 2 is a very versatile software, with numerous possible applications including hydrodynamic and morphodynamic modeling and even water quality and temperature calculations. For an extended analysis of all the files

utilized by the software Olsen's (2018) documentation of SSIIM is available. In Figure 2.11 the input and output files used by SSIIM 2 for the simulations of this thesis are shown.

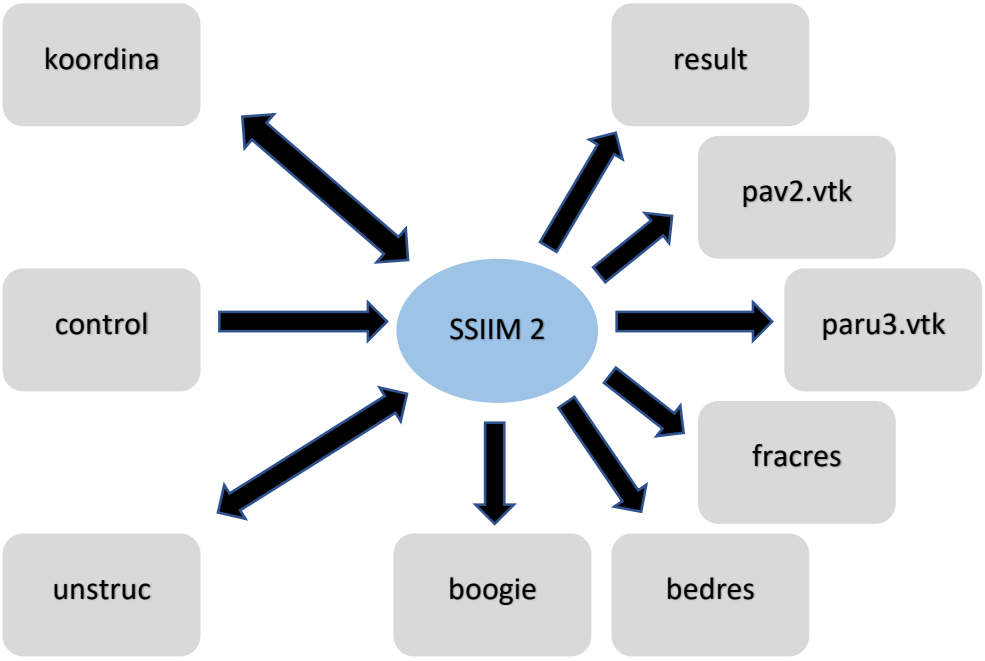

Figure 2.11 Input and output files used by SSIIM 2

The control file provides most of the parameters needed to set up the model. Using the available data sets, the algorithms used by the model for all the calculations are defined and their parameters are calibrated. Other than each case's geometry and initial water and bed levels, every other input the model requires is given through this file (e.g. the timestep, the sediment variables, etc.). This is the only file that is strictly an input file, SSIIM never writes on the control file.

The unstruc file contains all the information needed for the grid creation as well as the discharges at the inflows and outflows of the simulated reach. It is created by SSIIM 2 after defining the necessary parameters in the GUI. After its creation is serves as an input file.

The koordina file describes the riverbed geometry and when created by SSIIM 2 it also contains the initial water surface levels. After its creation it serves as an input file.

The result file contains the values of all the variables calculated for each cell. Those are the velocities, the k and ε values of the eddy-viscosity model and the pressure. Furthermore, it contains the fluxes on all the surfaces of the grid.

The pav2.vtk and paru3.vtk files are written in a Paraview compatible format and can contain a number of different variable values for each grid cell and point (grid line intersection) that can be then visualized in Paraview. All Figures used in the presentation and discussion of the results of this thesis are created using these files.

The fracres file contains the grain size distribution, given as a list of percentages of each sediment size, for every bed cell both for the active and the inactive layer as well as the thickness of each layer.

The bedrest file is similar to the fracres file, it contains the grain size distribution for every bed cell but it also contains the roughness and bed form height of the cells.

The boogie file is a general purpose file containing a lot of important information, mostly for troubleshooting when setting up the model. If no errors occur, the file only contains information about the grid, the algorithms used, the memory allocated, the initial values of parameters and the residuals for each of the six equations solved by SSIIM 2.

All the output files are printed out periodically after a number of iterations specified in the control file.

2.4 Linking grain size distribution with shelter abundance

By analyzing samples taken with the methods developed by Finstad et al. (2007) from the river Gaula in Norway Jocham (2010) established a correlation between some parameters derived from those samples and the number of crevices that can provide shelter for juvenile salmonids existing in the broader sampling area. The single square approach for the sampling (i.e. measuring shelter abundance and collecting the corresponding sediment samples from each square frame) yielded better results in Jocham's (2010) analysis..

First a quick overview of the parameters measured and calculated from the samples, using the single square approach, is given below.

By collecting and sieving the samples, cumulative masses of each grain size class are measured and cumulative frequencies are calculated. The percentile values of the samples are derived from this data. Percentile values indicate the percentage of the sediment sample that is finer than a certain grain size value. For example if the D_5 percentile of a sample is 5 mm, this means that 5% of that sample is finer than this value (has a grain size smaller than 5 mm). The percentile values are calculated from the cumulative frequencies using (2.15) (Bunte and Abt 2001).

$$D_x = (\log x_2 - \log x_1)\left(\frac{F_x - F_1}{F_2 - F_1}\right) + \log x_1 \tag{2.15}$$

Where D_x is the desired percentile. F_1 and F_2 are the cumulative frequency values calculated directly below and above the desired value. x_1 and x_2 are the particle sizes associated with F_1 and F_2. In Jocham's (2010) thesis all percentiles were calculated using φ units for the particle sizes, by using the Krumbein φ scale a logarithmic transformation is applied to the particle sizes. The transformation is shown in (2.16)

$$\varphi = -\log_2 \frac{D}{D_0} \tag{2.16}$$

Where φ is the particle size in the Krumbein φ scale, D is the particle size in mm and D_0 is a reference diameter equal to 1 mm used to make the equation dimensionally consistent (since φ units are dimensionless numbers)

For the grain size analysis carried out in this thesis all percentile values were calculated using particle sized in mm instead of φ units. The error induced by computing percentile values without a logarithmic transformation can maximally reach 1.7 % (Bunte and Abt 2001) which is of no significance for the purposes of this thesis' analysis of this parameter and by using a linear interpolation the method of calculating this parameter is simpler and more intuitive.

The significance and use of each percentile for establishing the desired correlation is described in Table 2.3.

Table 2.3 Percentile values and their significance (Jocham 2010)

Percentile Value	Significance
D_5	Characteristic percentile of the fine tail of the distribution, used as itself
D_{10}	Characteristic percentile of the fine tail of the distribution, used as itself
D_{16}	Statistically characteristic value, used to calculate parameters
D_{25}	Quartile, used to calculate distribution parameters
D_{50}	Median point, divides distribution in two equal halves
D_{75}	Quartile, used to calculate distribution parameters
D_{84}	Statistically characteristic value, used to calculate parameters
D_{90}	Characteristic percentile of the coarse tail of the distribution, used as itself
D_{95}	Characteristic percentile of the coarse tail of the distribution, used as itself

Another parameter measured on site for each sample is the number of available shelter providing crevices. A 0.25 m^2 square frame is tossed in random positions on the shore or in shallow water. In each square frame the total number of crevices is measured with a rubber

tube with a diameter of 13 mm. The crevices are then divided in three categories depending on their depth, first all crevices deeper than 3 cm are noted, then all the crevices deeper than 7 cm and then all the crevices deeper than 12 cm. An example is shown in Table 2.4.

Table 2.4 Shelter abundance example

Category	I (> 3 cm)	II (> 7 cm)	III (> 12 cm)
Number of shelters	5	0	0

The shelter abundance measurements were then plotted against percentile values and correlations between them were established by Jocham (2010). The only percentiles that have high coefficients of determination are the D10 and D_5, this means that the fine tail of the sediment distribution plays a major role in shelter abundance. The determination coefficients for each percentile are shown in Table 2.5.

Table 2.5 Determination coefficients for each percentile (Jocham 2010)

Percentile	**Determination coefficient R^2**
D_5	0.88
D_{10}	0.83
D_{50}	0.51
D_{90}	0.17
D_{95}	0.17

The total number of shelter plotted against the D_5 and D_{10} percentile values is shown in Figure 2.12

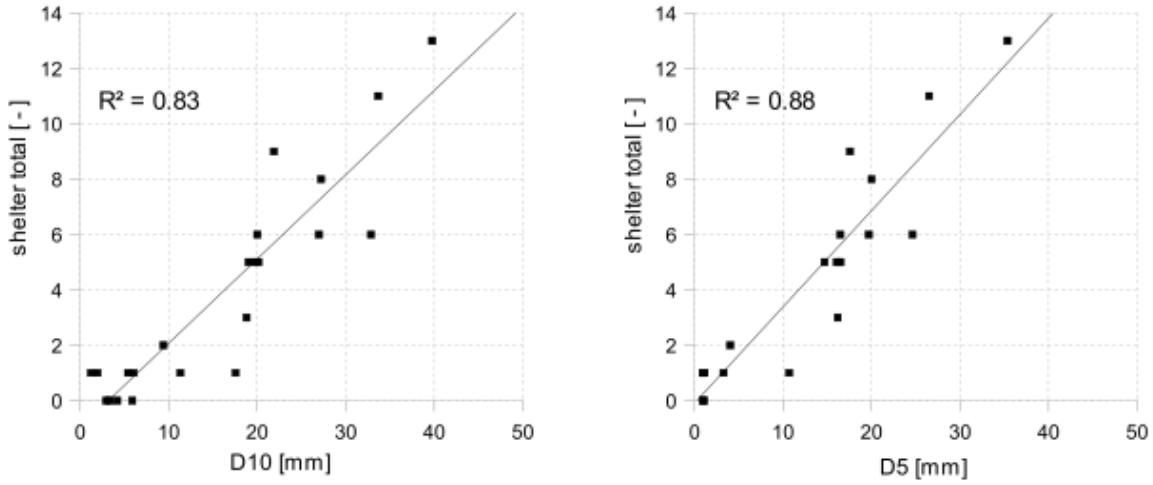

Figure 2.12 Shelter plotted against percentiles (Jocham 2010)

Another graph that is very useful for translating sediment parameters, the D_5percentile in this case, to shelter abundance is that of the per shelter number averaged D_5percentile plotted against the number of available shelter, shown in Figure 2.13. Averaging the D_5values per shelter number leads to a very linear dependency ($R^2 = 0.93$) between the 2 variables. This graph combines measurements from both the single and multi-square approach.

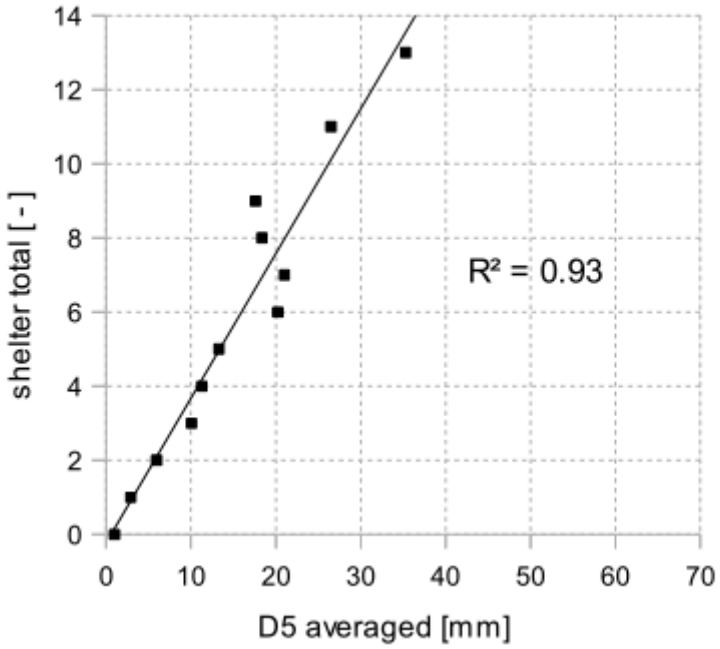

Figure 2.13 Per shelter number averaged D_5 percentiles plotted against the number of available shelters (Jocham 2010)

The data points follow the regression line almost perfectly in the lower region of the graph (D_5 smaller than 15 mm and less than 5 shelter crevices measured) and even though at the upper region the data points slightly deviate from the line, this analysis of the measured variables gives the most linear dependency between them compared to any other analysis tried by Jocham (2010).

2.4.1 Conversion of substrate conditions to shelter abundance map

Using the data from the fracres output file from SSIIM the sediment curve at the end of the simulation is calculated for each bed cell of the grid. The D_5 percentile is then calculated using equation (2.15). The final D_5 values are then compared to the initial ones to give an overview of how the substrate conditions, more specifically the critical parameter for shelter abundance, were affected by the simulated event. Then the available shelter is calculated using the linear equation plotted in Figure 2.13 and is displayed on a map of the reach geometry. This linear correlation between the D_5 percentile and the available total shelter was chosen because it has the highest coefficient of determination of all the plots derived by Jocham's (2010) analysis.

The data manipulation mentioned above was done using a Matlab script, shown in Appendix B.

3 Sensitivity analysis

The nature of the result analysis in this thesis is comparative. Comparing the results of the case using the measured sediment data with the results of the artificially created cases (different substrate compositions and sediment inflow). Mainly with the goal to assess how shelter abundance is affected by different sediment regimens. Even though fidelity to the real events described is a requirement of any simulation, hydraulic or otherwise, in these cases the calibration of the model using measured data for the simulated discharge was not possible because no such data was available. But seeing that the goal, as described above, is the comparison of results between different simulations using the same model; an initial calibration of the bed roughness parameter k_s and a subsequent sensitivity analysis of some of the models parameters, further discussed below, was deemed enough for the model to be useful this objective.

3.1 River bed roughness

The velocity data used for calibrating the bed roughness were measured using an ADCP (Acoustic Doppler current profiler) instrument creating 26 cross-sectional profiles in the simulated river reach. The discharge of the residual channel on the day of measurement was around 10 m^3/s. This gives vastly different flow conditions from the discharge used for the cases analyzed in this thesis, but simulations were run with a 10 m^3/s discharge to decide the bed roughness. The initial bed roughness used by SSIIM by default is equal to 3 D_{90}, for the reach's bed composition that is 29 cm. Comparing the measured velocity vertical profiles with simulated ones for values of the k_s parameter ranging from 29 to 45 cm showed that a bed roughness of 40 cm gives the best results. This value is very high, especially when the physical representation is taken into consideration, since there are areas near the banks with water depth smaller than 40 cm. Nonetheless it is acceptable as it is primarily used as a sink term for the velocities near the river bed.

3.2 Iteration parameters

After setting up the physical parameters of the model, a sensitivity analysis of some of the parameters concerning the numerical simulation was done. The goal of this is the

optimization of the model with regard to computational time and resources without affecting the results. The parameters taken into consideration were:

- The time-step
- The number of inner iterations for each time-step
- The number of iterations for sediment calculations

3.2.1 Time step

The parameter with the biggest impact on the computational time needed is the time step. Two different time steps were considered, 10 and 20 seconds. For simulating the same 24-hour period the computational time needed is almost halved when the time step is doubled. The result output interval was set to 1000 seconds in both cases, meaning that the volume of results that are available for analysis is not reduced when doubling the time step. This has minimal impact on the computational time.

In the cases using Curve 1 as the initial river bed sediment composition, both with and without sediment inflow, the time step had very little impact on the results. For the case with no sediment inflow, compared to the results given with the 10 second time step, using a 20 second time step slightly underestimated the bed shear stress, seen in Figure 3.1. The effect the different time step had in the estimated shelter abundance is shown in Figure 3.2.

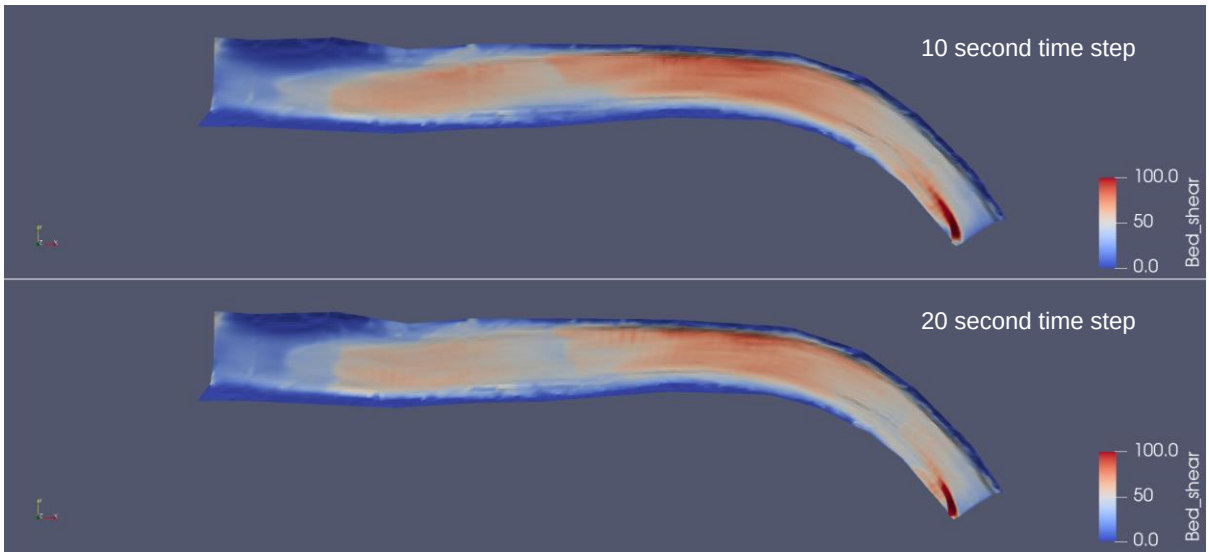

Figure 3.1 Bed shear stress: Curve 1, no sediment inflow.

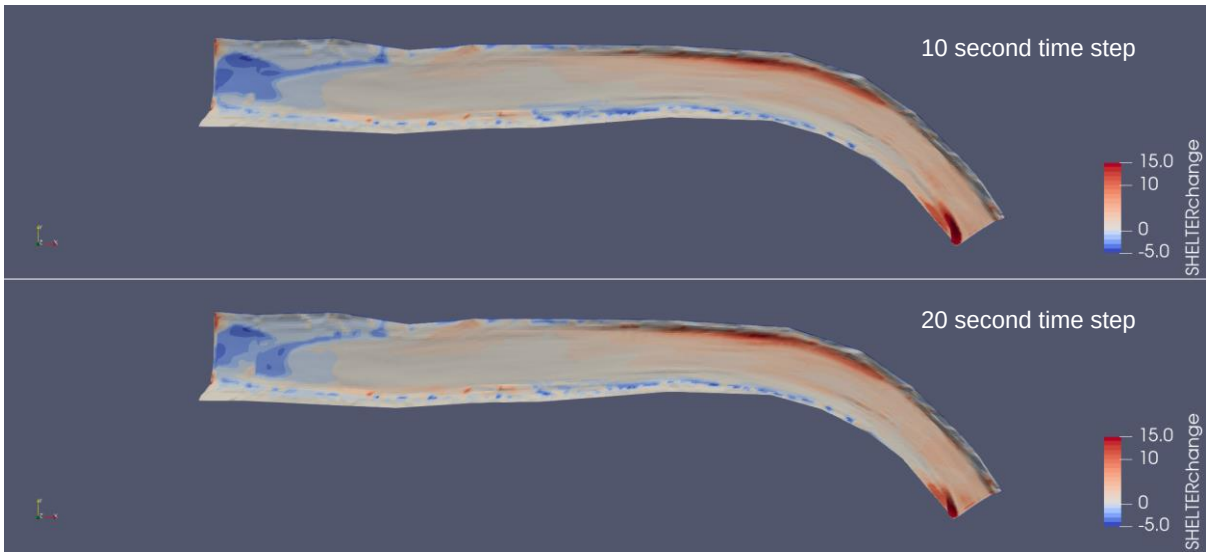

Figure 3.2 Change in number of shelter compared to initial conditions: Curve 1, no sediment inflow

The same effects are also observed in both the cases with sediment inflow, an underestimation of the bed shear stress resulting in slight differences in the estimated shelter abundance. In the case with the fine sediment inflow, there is a pattern of overestimating the positive change in shelter abundance while underestimating the negative change when using a 20 second time step compared to a 10 second time step. This can be seen in Figure 3.3, where the area with reduced shelter abundance near the downstream boundary is smaller and the area of increased shelter abundance near the upstream boundary is more prominent.

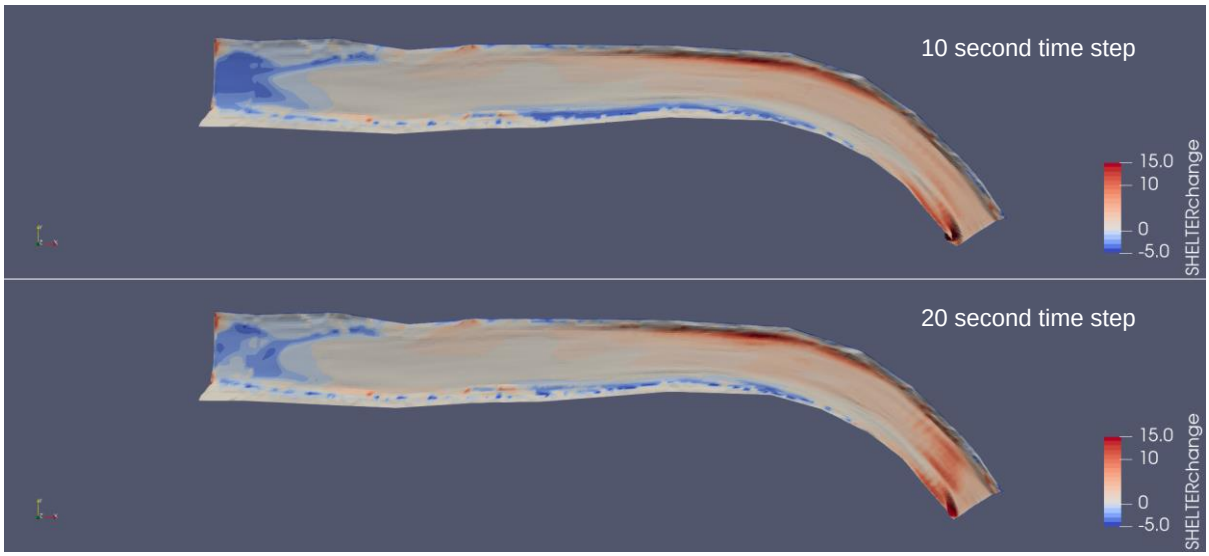

Figure 3.3 Change in number of shelter compared to initial conditions: Curve 1, fine sediment inflow

The same pattern is seen in the simulations using the artificial sediment curves as initial substrate conditions. A slight underestimation of bed shear stress by the simulations using a 20 second timestep with small impact on bed movement and shelter abundance.

3.2.2 Inner iterations

The number of inner iterations are done by the algorithm for each timestep also has a big impact on computational time. The main reason for increasing the number of inner iterations, at the expense of computational time, is to improve convergence and stability of the solutions. The residuals for all 6 main equations solved by the model the final outer iteration are the same for all three values of inner iterations used (200, 250 and 300). With the highest one being the residual of the pressure equation, at 1.9×10^{-3} for all three. The residuals regarded are the highest residuals for each equation in all the cells of the computational grid for the given timestep. This means the model converges, with residuals on the scale of 10^{-3} even for 200 inner iterations per timestep. The pressure residuals for the first 100 outer iterations (using a 10 second timestep) are shown in Figure 3.4, none of the 3 values seem to give better results for initial convergence and the same is observed for the rest of the simulation.

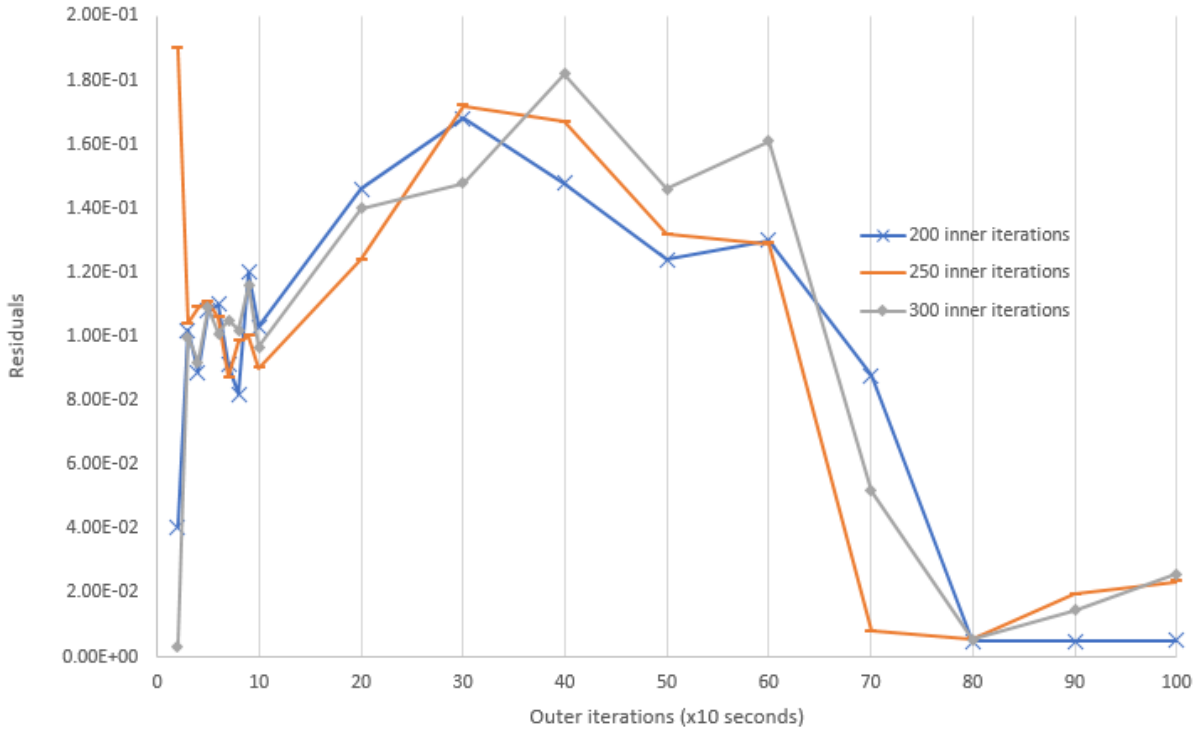

Figure 3.4 Pressure residuals for different values of inner iterations

Residuals of the velocity equations were much lower, on the scale of 10^{-5} for the first 100 outer iterations and reaching 10^{-7} at the end of the simulation. This is also unaffected by the values of inner iterations used.

The residuals followed the same pattern for the 20 second timestep. Concluding that using more than 200 inner iterations per timestep does not affect the convergence of the results or its stability.

3.2.3 Sediment calculation iterations

The number of iterations used for solving the sediment bedload equation is very small compared to the hydrodynamic equations, since they are not as complex. This means it has a smaller impact on computational time

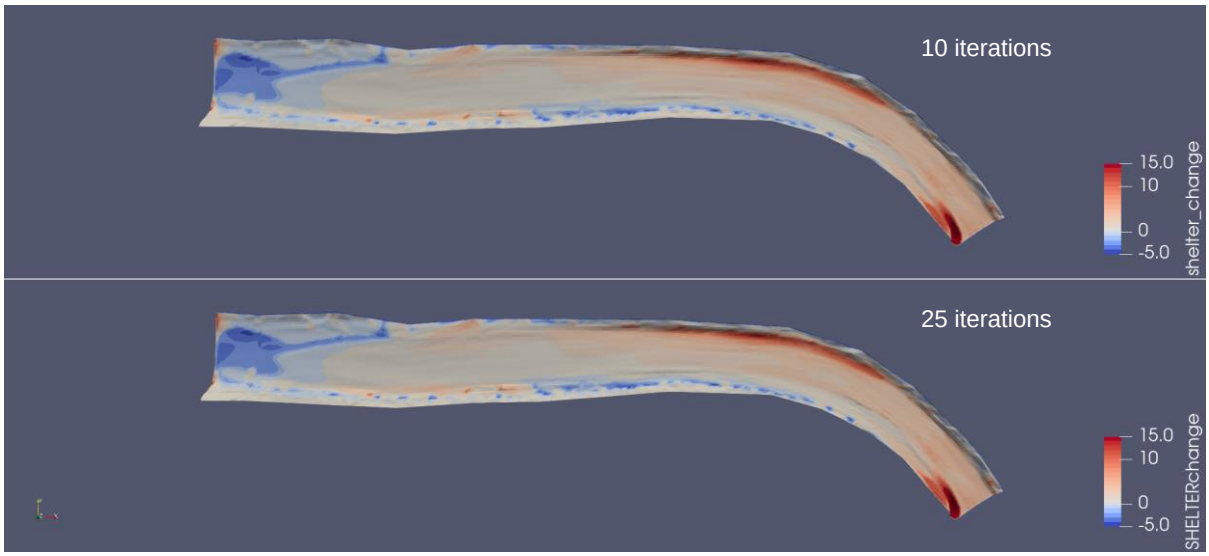

Figure 3.5 Change in number of shelter compared to initial conditions: Curve 1, no sediment inflow

Two different values for the sediment load iterations were considered, 10 and 25. Increasing the value of this parameter from 10 to 25 had no impact on the results. It is clear in Figure 3.5 that the resulting change in shelter abundance on the river bed is estimated to be exactly the same in both simulations. It is then concluded that increasing the number of sediment load calculation iterations serves no purpose in the scenarios simulated in this thesis and only increases computational time.

4 Results

The numerical model was applied to the computational grid with a discharge of 100 m^3/s and 3 different substrate compositions simulating a 24-hour event. Two cases where the inflow discharge is infused with different mixtures of sediments were also simulated to examine the results of artificial inflow of sediment in the reach. The first sediment mixture introduced serves as an example of a favorable sediment inflow with regards to potential shelter abundance change in the reach, consisting of relatively coarse grain sizes (with a mean value of 22.6 mm). The second sediment mixture serves as an example of an unfavorable inflow, consisting of relatively fine grain sizes (with a mean value of 9.7 mm).

The parameters that are of interest can be divided in two categories, those describing the conditions on the river bed and those describing the flow field

With regards to the waterflow, the parameters that are examined are:

- The water depth
- The average water velocity for each water column

With regards to the river bed, the parameters that are examined are:

- The sediment grain size composition, defined by the percentile values for each cell, and specifically the D_5 value given the high correlation it has with shelter abundance.
- The changes in geometry due to erosion and deposition
- The shear stress calculated on the river bed, seeing that this is the driving factor behind the processes of calculating erosion and deposition. Creating in turn the changes in grain size composition.

The following analysis and discussion is mainly focused on the conditions resulting in the reach after a simulated 24-hour period of steady discharge. All figures used that do not state otherwise are representing this state of quasi-steady flow (since the bed morphology is changing, achieving steady flow conditions is not possible) resulting after the 24-hour period simulated. But in some instances (especially in the cases where sediment mixtures are introduced), an overview of the development of the results over time gives additional

information and insight into the sedimentation process. When results from different points in time than the final stage are examined, the time elapsed since the simulation commencement is noted on the figure in seconds.

The simulations for all scenarios encountered some computational problems on the left hand side of the inflow cross-section, as a consequence the variables calculated at this specific spot do not correspond to reality. In that spot the velocity and shear stress on the bed are very high, causing a lot of erosion and depositing most of the eroded material directly downstream of the inflow boundary resulting in very big bed changes and also changes in the sediment composition and shelter abundance. This does not affect the rest of the results in any major way and hence the irregularities on that spot will not be examined when interpreting the results.

Here it is noted again that the orientation in the computational grid is maintained from the original georeferenced geometrical data, with the waterflow in this part of the river being from east to west. This means that in all the figures the inflow boundary is on the right hand side and the outflow boundary on the left hand side, with water flow and sediment movement occurring from right to left.

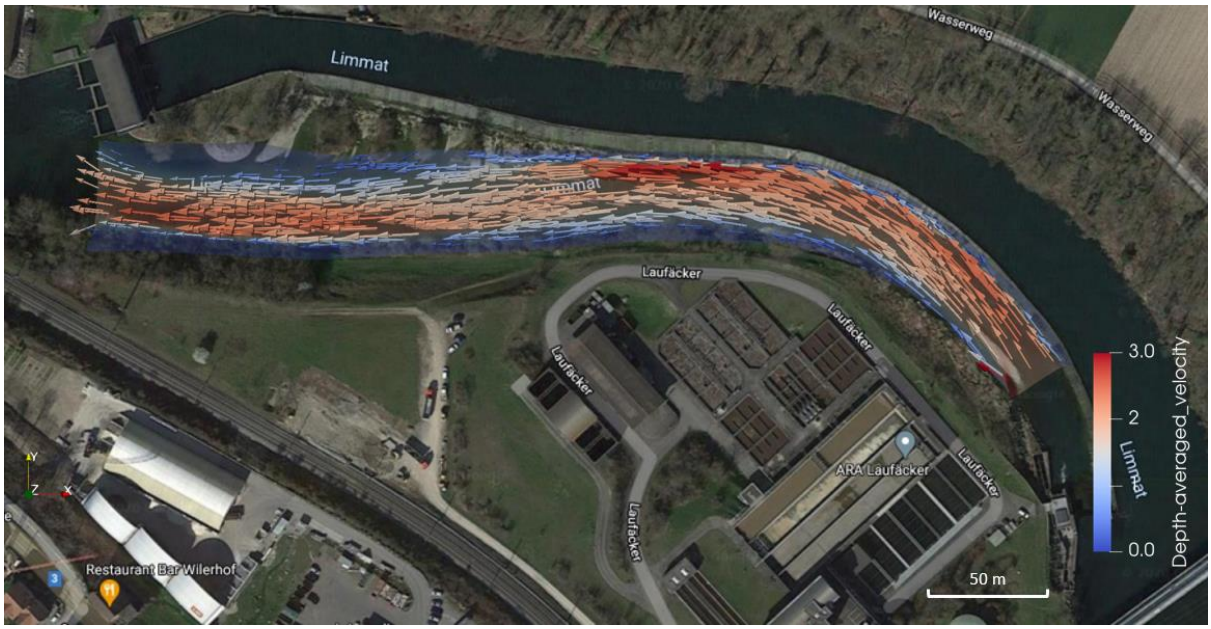

Figure 4.1 Waterflow visualized with velocity vectors.

The results are presented below, first for the simulations with no sediment inflow and then for the different sediment inflow scenarios.

4.1 Scenarios with no sediment inflow

The interpretation of the results of these simulations serves two purposes, seeing the impact a high discharge event has on the reach and more specifically the shelter abundance for juvenile Atlantic salmon and also giving a baseline measure against which to compare and better evaluate the results of the scenarios where sediment is introduced to the reach.

4.1.1 Scenario 1: Measured sediment curve as initial substrate conditions

In this scenario the grain size curve derived from the field measurements (Curve 1, Figure 2.8) was used to set the initial sediment distribution on the river bed. The initial value of the D_5 percentile is 15.2 mm, giving an initial value of 6.3 (crevices measured with the Finstad method) for shelter abundance.

The water depth reaches up to 3 meters near the downstream boundary, where the bed is less steep. In the rest of the reach the water depth is around 2 meters with a shallow water area (less than 1 meter) existing on the inside part of the bend (light blue area seen in Figure 4.2).

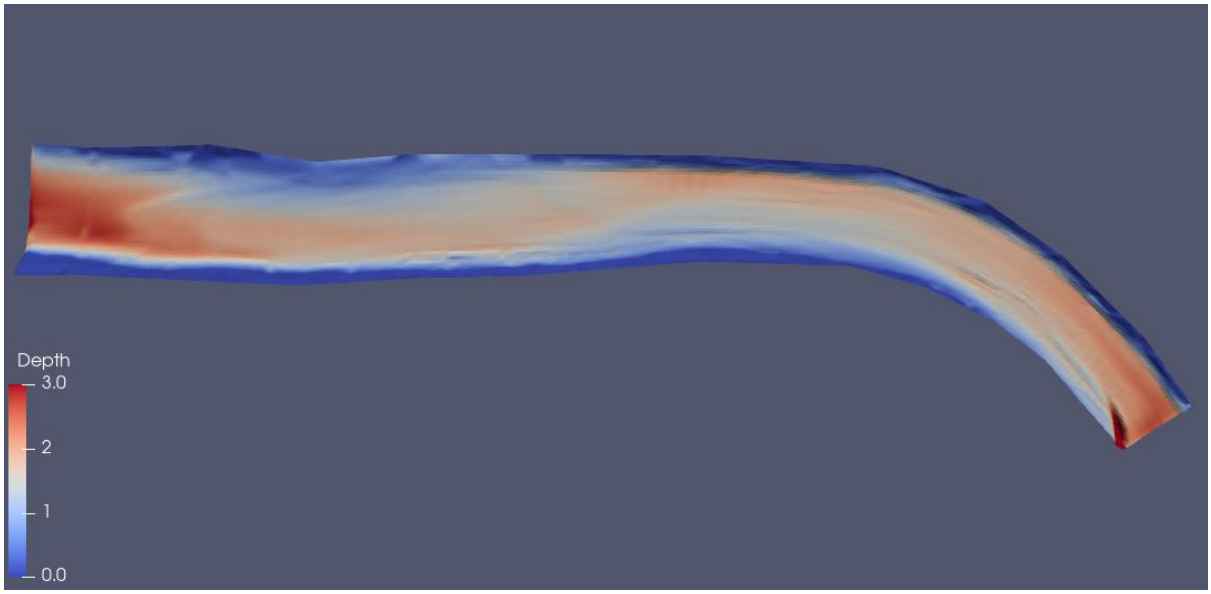

Figure 4.2 Water depth: Scenario 1

The velocities developed in the stream as represented by their depth averaged values are shown in Figure 4.3. The magnitude of the water column velocities ranges up to 3 m/s in the more rapid sections of the stream, on the outside part of the bend and near the left bank directly upstream of the outflow boundary, with the flow slowing down when the water depth is reduced near the natural banks of the reach. In the former section the velocities calculated at the cells nearest to the bed are between 2 and 3 m/s while in the latter they only reach up to 2.5 m/s. On the outside part of the bend the boundary is a steep concrete wall separating the simulated reach from the river segment utilized by the HPP, allowing for high water depths and velocities to occur as opposed to the natural river banks.

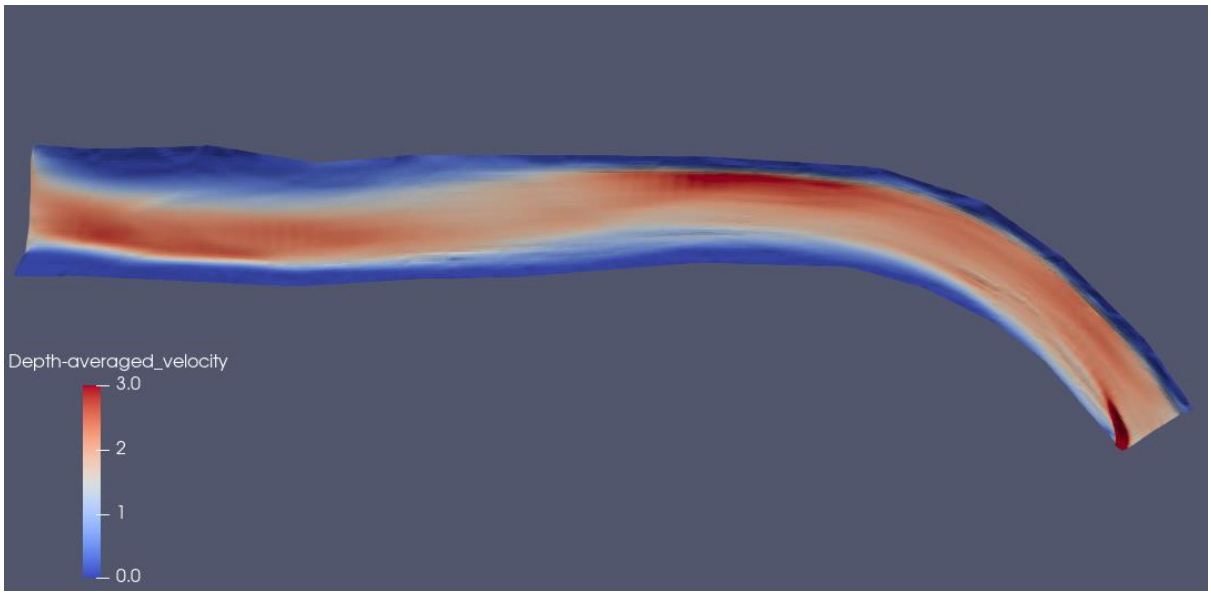

Figure 4.3 Depth averaged velocities: Scenario 1

Shear stress is the determining factor for incipient motion of sediment grains, which is determined by calculating the critical shear stress for each grain size using (2.9) and then comparing it to the effective bed shear stress.

The maximum shear stress is about 90 Pa, occurring on the outside part of the bend, slightly upstream the middle of the simulated reach at the areas with the highest water velocities.

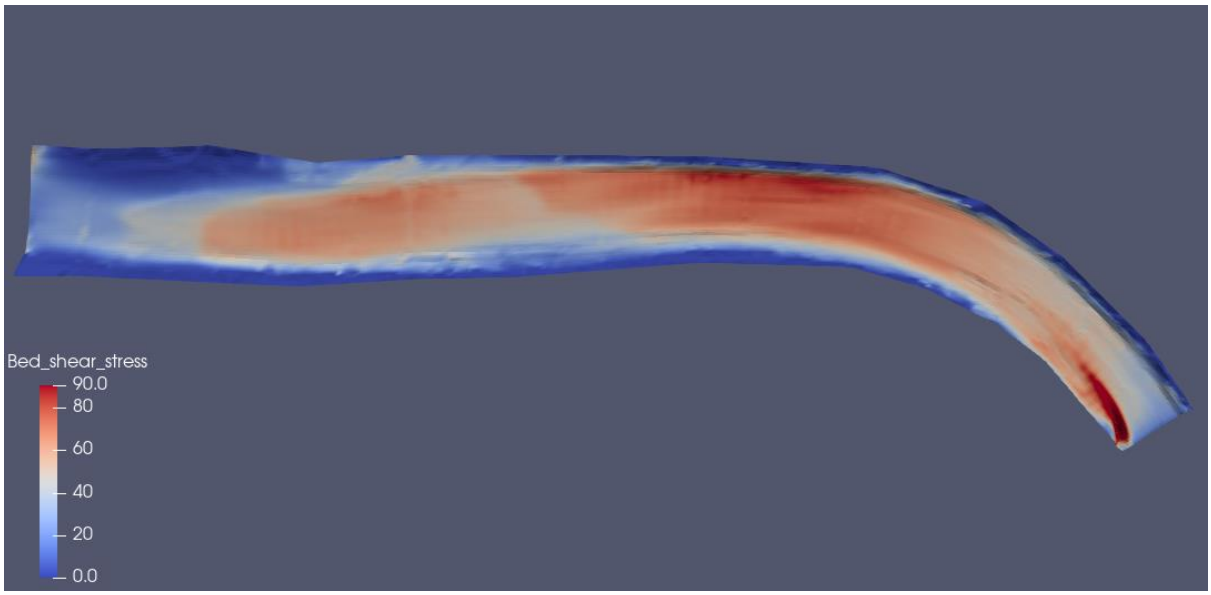

Figure 4.4 Bed shear stress: Scenario 1

By solving (2.9) for τ_c, the critical bed shear stress for incipient motion and then applying it to (2.10) neglecting the effective shear velocity reduction because of the Chézy coefficient we can see that cobble with diameters of up to 12 cm is estimated to start slipping in that area. This quick calculation slightly overestimates the maximum diameter of sediment that gets moved by the flow but serves as an easy rule of thumb to indicate that according to the model no cobble with diameter larger than 12 cm passes the threshold of incipient motion. The shear stress gradually decreases around this area but still stays high enough to ensure incipient motion for cobble with a diameter of 8 cm in that section of the reach. Near the outflow boundary, in the area where the biggest values for the water depth were observed, the shear stress at the bed is very low.

The shear stress calculated on parts of the river bed is sufficient for moving substantial amounts of sediment causing erosion and deposition of a part of that material.

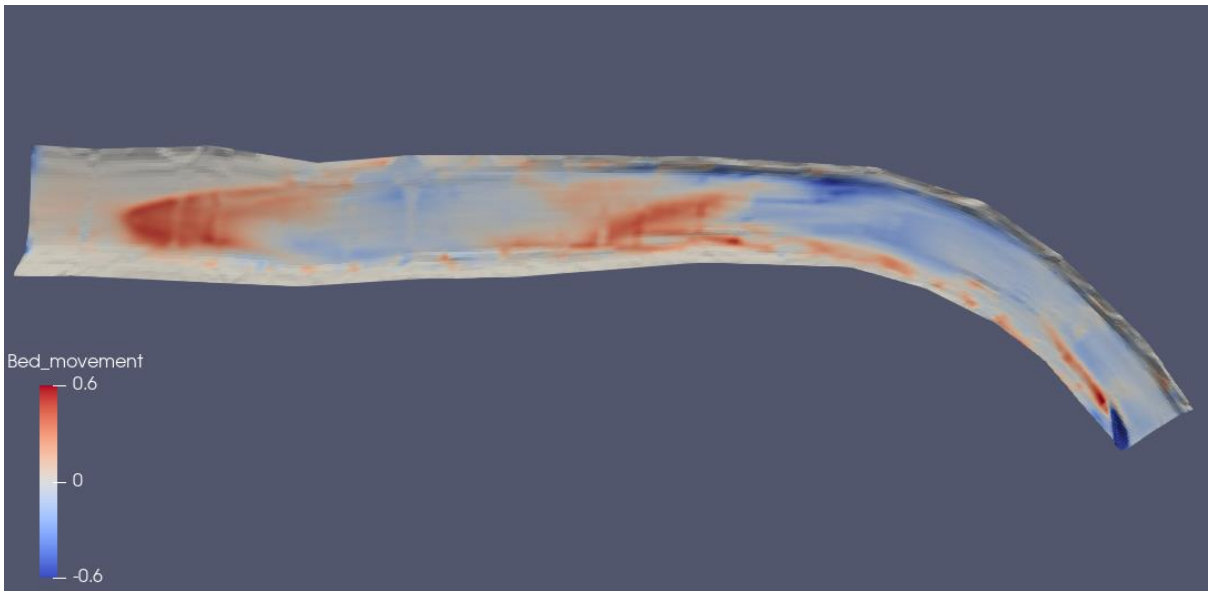

Figure 4.5 Bed movement: Scenario 1

Areas where erosion has occurred are seen in blue in Figure 4.5, the main one being the high velocity, high shear stress area on the outside of the bend where the bed level is lowered by 0.6 m in 24 hours. Two main deposition areas were created, one directly downstream of the main erosion and one in the low shear stress area near the outflow boundary.

Even though the initial substrate composition follows the measured substrate conditions of the reach (Curve 1, Figure 2.8) , which is a mixture of fine and coarse material, and is spatially homogeneous; the sediment movements described above have an effect on the resulting substrate conditions. Not only changing the geometry of the river bed but also the distribution of sediment, by way of uneven sediment movement for different grain sizes the resulting substrate composition, after the simulated 24 hours, differs from area to area. This leads to the estimated shelter abundance also being affected and made spatially non-homogeneous. The change in number of estimated shelter that occurred in the 24 hour simulated event is shown in Figure 4.6. The initial calculated shelter abundance was 6.3 crevices/0.25 m^2 (following the Finstad method), the resulting shelter numbers range from 2 to 20. Two areas of significant shelter change were created, one on the outside of the bend and one directly downstream from the big deposition dune seen in Figure 4.6. In the first area shelter

abundance was vastly improved while on the second one available shelter almost disappeared as the D_5 percentile was lowered significantly.

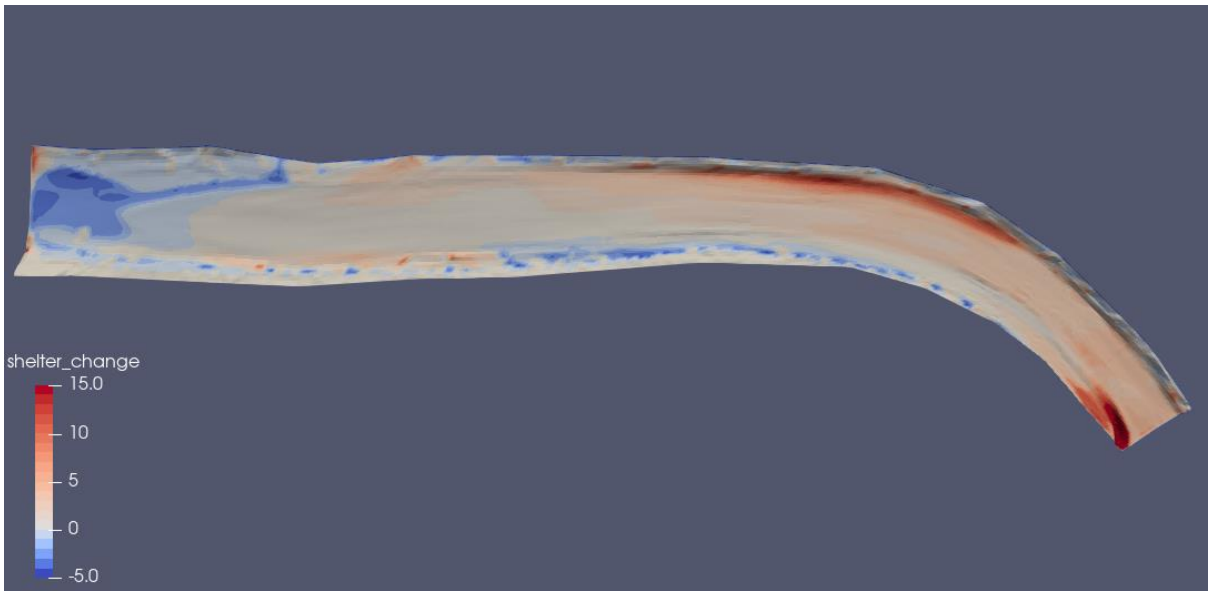

Figure 4.6 Change in number of shelter compared to initial conditions: Scenario 1

In the biggest part of the river bed, only small changes are seen in this parameter. Outside of the two areas described above, shelter abundance was very slightly improved in the entirety of the river bed. This can be seen in Figure 4.7 where the data range coloring is changed to better illustrate small changes in the parameter. This happens because in the areas where no big bed movements occurred, only a small amount of fine sediment was eroded from the top layer of the substrate resulting in a slight increase of the D_5 percentile which is in turn translated to small shelter abundance improvements.

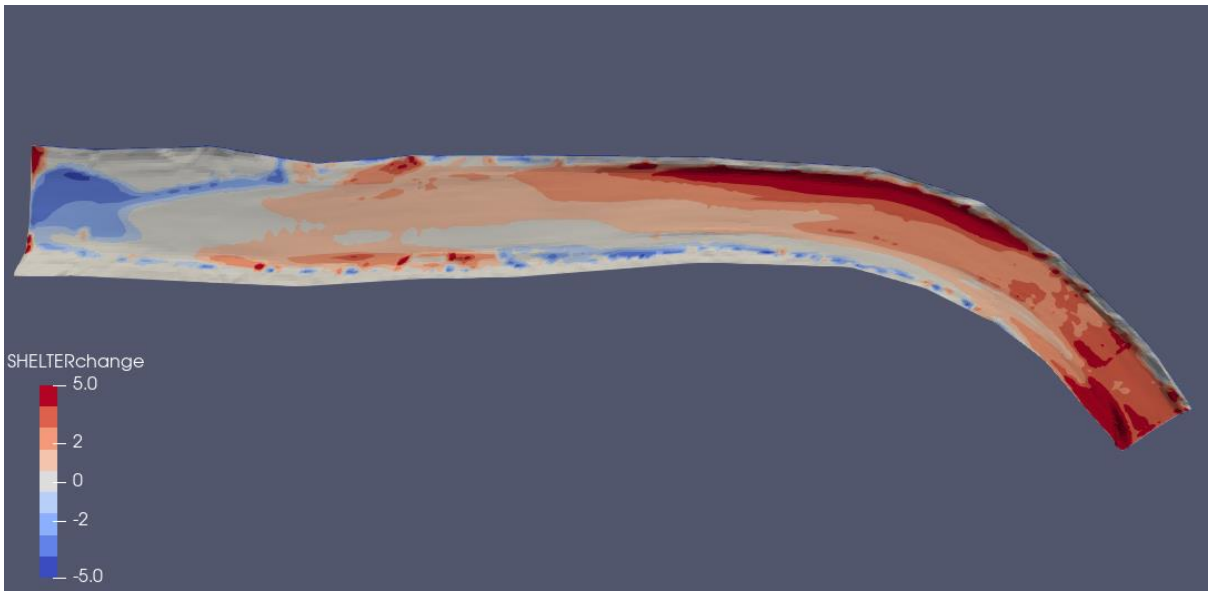

Figure 4.7 Change in number of shelter compared to initial conditions: Scenario 1 (modified colour map)

4.1.2 Scenarios 2&3: Artificial sediment curves as initial substrate conditions

The second sediment curve comprises exclusively of fine sediment, with 90% of the sediment grains being smaller than 15 mm in diameter. This results in a very easily erodible bed. This artificial substrate scenario was simulated to see how the shelter abundance in a reach with this bed composition would be affected by a high discharge event.

The third curve is also heavily skewed towards the fine side, comprising mainly of gravel similar to the second curve but also adding cobble to the mixture. The D_{90} of this sediment curve is 63 mm. The main difference between the two mixtures is that the third one incorporates a wider range of grain sizes, ranging up to 170 mm, resulting in a non-uniform sediment grain transport from the waterflow.

The D_5 for the second and third curve is respectively 4.2 and 4.3 mm, resulting in an initial value of 2 crevices for shelter abundance (following the Finstad method).

In both scenarios the water depth is significantly bigger than the scenario using the original sediment curve. The bed is more erodible resulting in a lot of sediment getting flushed in the areas where the water creates strong shear stresses near the bed boundary, this in turn creates areas of deep flow (mainly on the outside part of the bend where higher velocities

appear). This creates a very shallow water region at the inside part of the bend, more prominently in Scenario 2, as seen in Figure 4.8. In Scenario 2 the water depth reaches 7 m in the deep flow area described above and maintains a depth of around 3 m in the rest of the reach with the flow following a meandering curve. In Scenario 3 the water depth is more uniform throughout the reach at 3 m, ranging up to 4 m in the deeper parts on the outside of the bend.

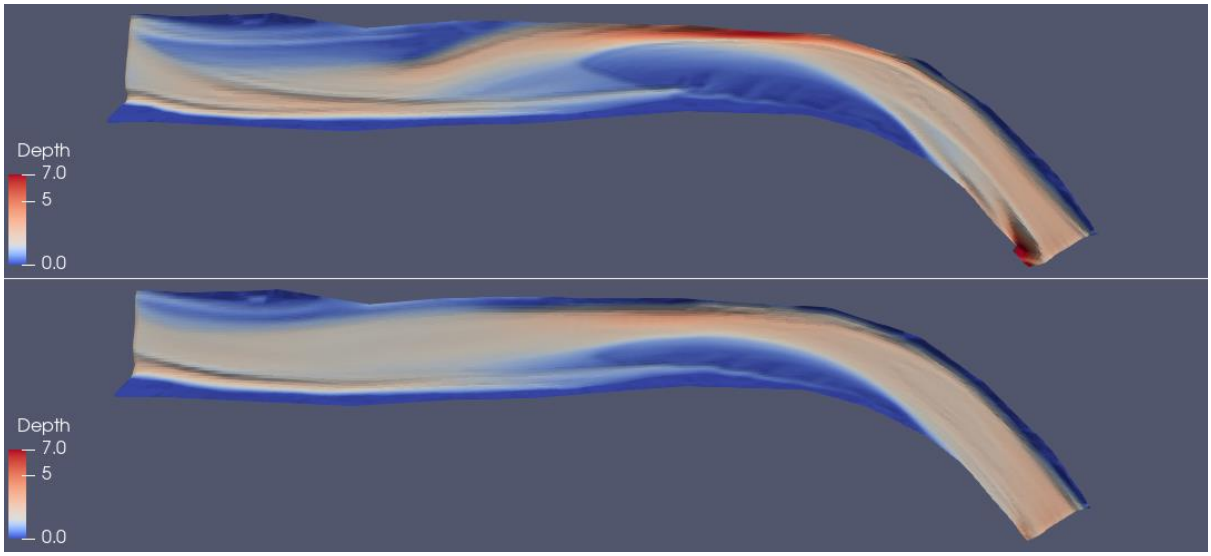

Figure 4.8 Water depth: Scenario 2 (top) and Scenario 3 (bottom)

Due to the narrowing of the flow at the bend the mean water column velocities are high in that region, reaching 8 and 5 m/s in Scenarios 2 and 3 respectively. The velocities in the rest of the reach are between 2 and 3.5 m/s in both Scenarios.

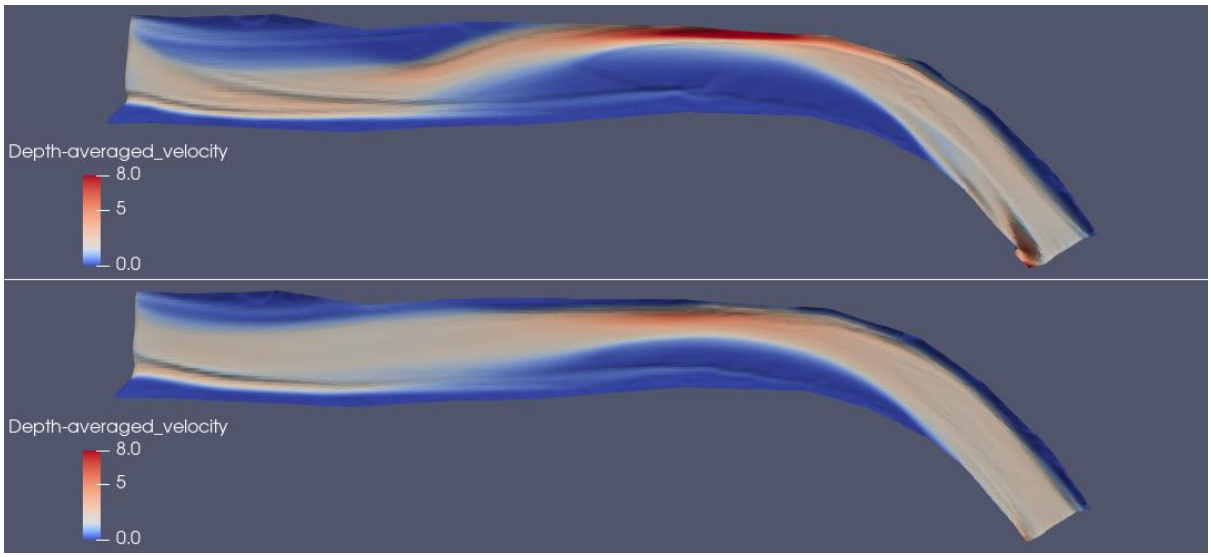

Figure 4.9 Depth averaged velocities: Scenario 2 (top) and Scenario 3 (bottom)

The bed shear stress is relatively low in the biggest part of the reach in both Scenarios. In Scenario 2 it ranges from 30 to 70 Pa. In Scenario 3 an area of high shear stress is created on the outside part of the bend, taking values up to 85 Pa. In the rest of the reach the shear stress is calculated to be below 60 Pa. Even though the values are lower than those of the first Scenario they are enough to cause incipient motion in big parts of the river bed due to the fine sediment composition of the bed.

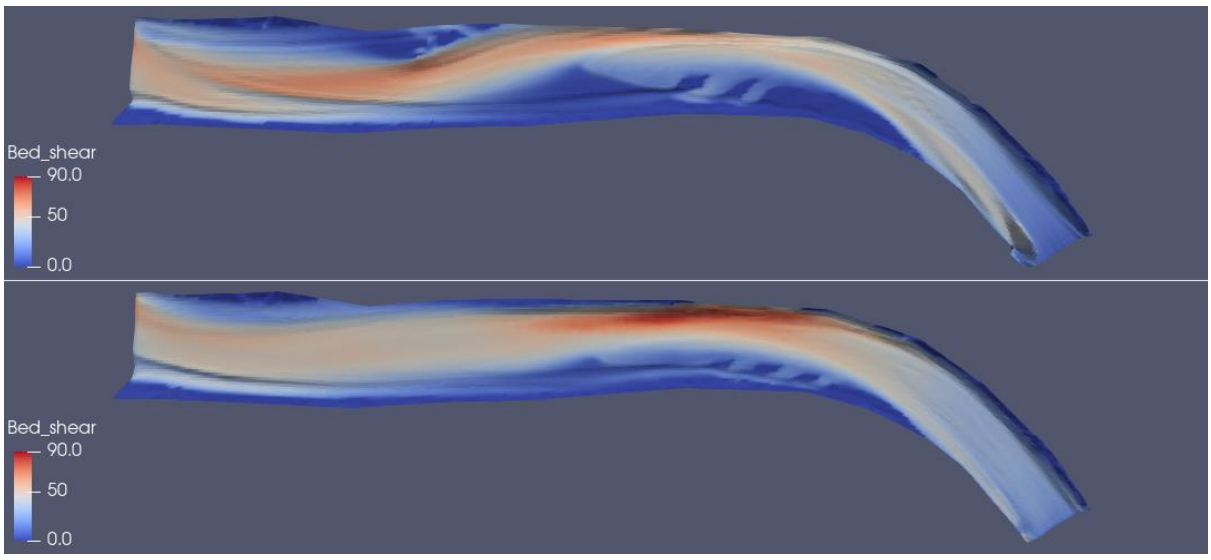

Figure 4.10 Bed shear stress: Scenario 2 (top) and Scenario 3 (bottom)

Both scenarios result in significant bed movements, with erosion being in general more prominent than deposition. In Scenario 2 up to 5 m of sediment are eroded in the high velocity area described above, smaller degrees of erosion are also seen in the upstream section of the reach. Part of the eroded sediment is flushed by the flow and part of it is deposited in the low depth/low velocity area at the inside of the bend and near the outflow boundary. In Scenario 3 a similar pattern of deposition is observed; while the level of erosion is not as high, reaching a depth of 2.5 m.

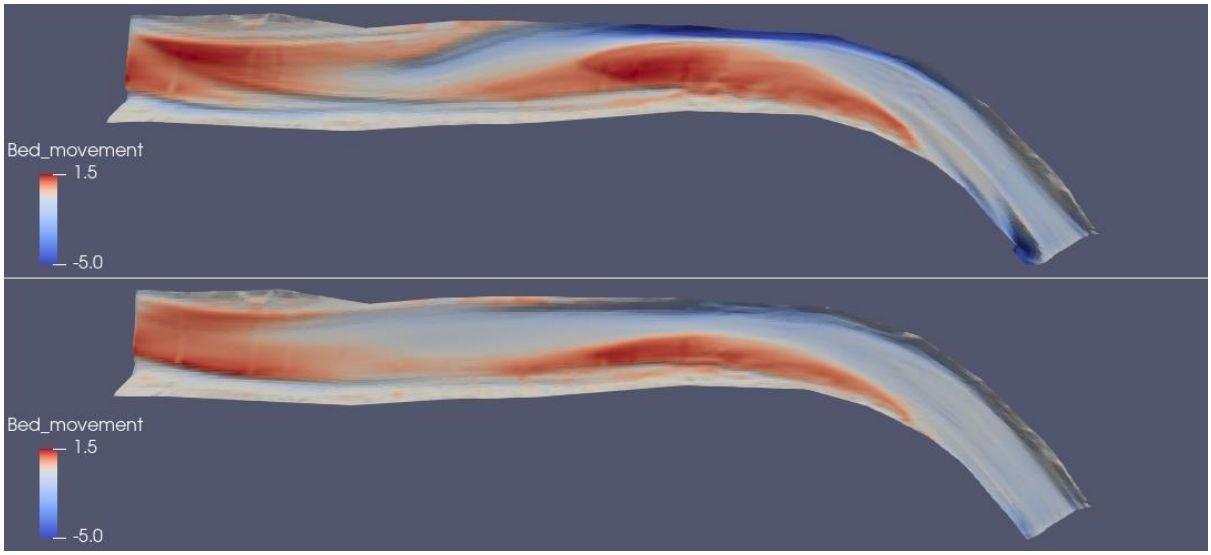

Figure 4.11 Bed movement: Scenario 2 (top) and Scenario 3 (bottom)

As noted above, while the bed shear stress is lower than that developed in the first Scenario, it is sufficient for incipient motion of the fine sediment that comprises the river bed in both Scenarios 2 and 3. The bed in the second Scenario is comprised exclusively by fine sediment (with a D_{90} of 15 mm), this results in a uniform erosion and deposition with regards to the grain sizes. This means that the flow moves the sediment without separating fine from coarse grains, so unlike the first Scenario the percentile values of the sediment distribution are not changed. This is displayed in Figure 4.12 (top), the shelter availability has not changed since the D_5 is not affected by the sediment movements.

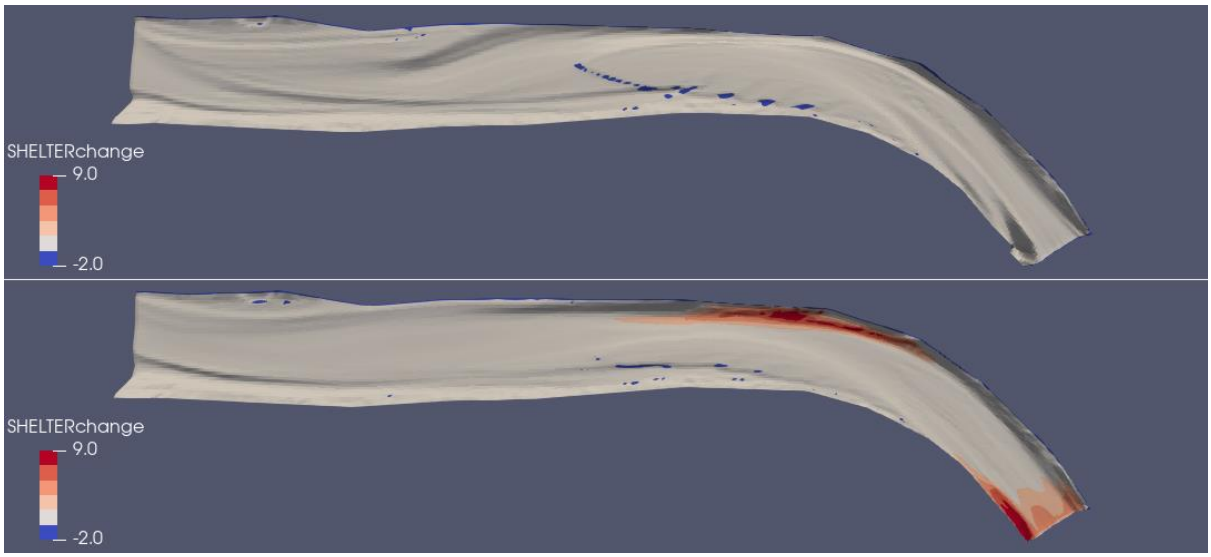

Figure 4.12 Change in number of shelter compared to initial conditions: Scenario 2 (top) and Scenario 3 (bottom)

In the third Scenario an increase in shelter availability is predicted near the inflow and on the outside part of the bend. This is likely due to the fact that the bed in the third Scenario also comprises of some coarse material, resulting in a separation of fine and coarse grains in some areas causing the percentile values of the sediment grain size curve to change. However, no reduction in shelter availability is predicted.

4.2 Scenarios with sediment inflow

Two scenarios with sediment inflow were simulated using the initial conditions of Scenario 1 and a ninety-minute inflow of sediment that commences at the beginning of the simulation. The composition of the sediment introduced in these scenarios (Scenario 4 and 5) are shown in Table 2.2. The mixture used in Scenario 4 aims to improve the substrate conditions for juvenile Atlantic Salmon shelter, while the mixture used in Scenario 5 simulates an inflow of fine sediment into the reach that if not flushed away is expected to decrease shelter availability.

Seeing that both Scenarios with sediment inflow have the similar initial and boundary conditions to Scenario 1 (only adding a relatively small quantity of sediment for a brief time in each case) the resulting waterflow parameters are expected to be almost identical to those

of the first Scenario. Those parameters, i.e. water depth and depth-averaged velocity, are shown for both Scenarios in Figure 4.13 and Figure 4.14 respectively.

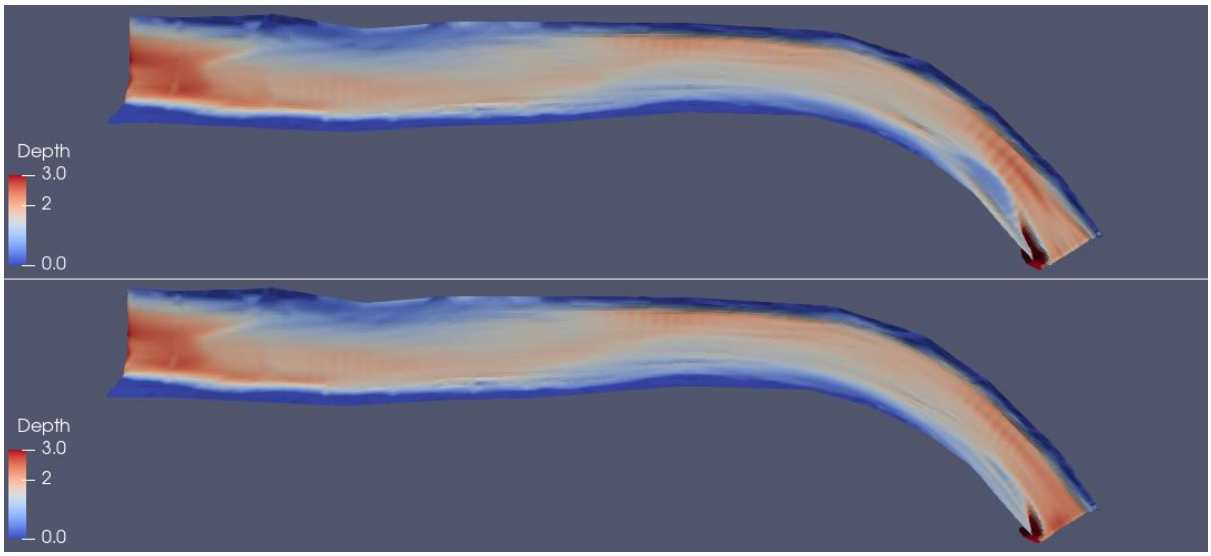

Figure 4.13 Water depth: Scenario 4 (top) and Scenario 5 (bottom)

The computational anomaly at the inflow created a lot of erosion and a subsequent deposition dune in both these Scenarios, especially Scenario 4. This should not be taken into consideration when interpreting the results. In all parts of the reach except for the area on the left hand side of the inflow boundary described above it is indeed the case that the calculated water depth in Scenarios 4 and 5 is almost identical to that of Scenario 1. The water depth is below 3 m in the whole reach. The deep part of the flow follows the meandering geometry of the river, with water depths around 2 m and shallow parts on the insides of the flows curves. As in the first Scenario, the biggest depths occur near the downstream boundary of the reach.

The same similarities to the first Scenario are also observed for the calculated mean water column velocities. The depth averaged velocity ranges up to 3 m/s in the rapid section of the flow on the outside of the bend, while having values between 1.5 and 3 m/s in the rest of the main flow areas.

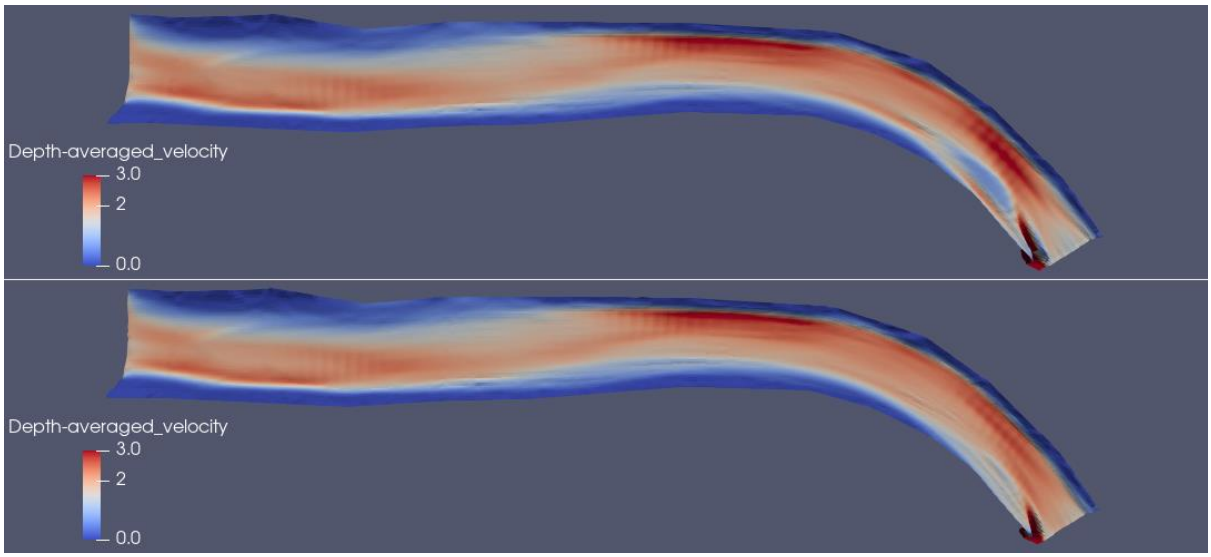

Figure 4.14 Depth averaged velocities: Scenario 4 (top) and Scenario 5 (bottom)

The bed shear stress values in Scenarios 4 and 5 are similar but slightly higher than those resulting from Scenario 1. The shear stress reaches 90 Pa after the inflow and at the main bend of the reach and it decreases further downstream where velocities are also decreasing. Near the outflow boundary the shear stress on the bed is very low, this is consistent with the first Scenario and also with the increased depth at that area.

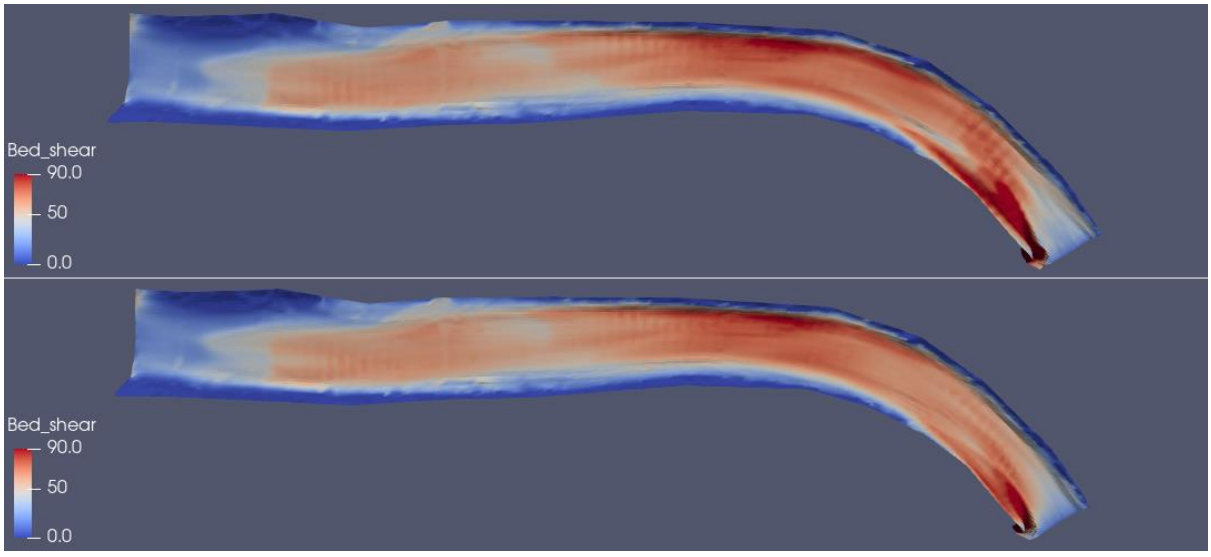

Figure 4.15 Bed shear stress: Scenario 4 (top) and Scenario 5 (bottom)

The phenomenon simulated in Scenarios 4 and 5 —the inflow of sediment for a brief time and its subsequent flushing— is a transient one. The goal is to assess if the shelter availability is affected by this phenomenon after the 24-hour simulated period but to understand the process undertaken it is helpful to examine results from different timesteps during the simulation. The water inflow is infused with sediment for the first 5400 seconds (90 minutes) in both Scenarios, to capture the sediment "wave" created by this the resulting bed changes and available shelter from 4 different timesteps (5th, 10th, 15th and 20th) are presented below, as well as the figures for these parameters' results at the end of the simulation.

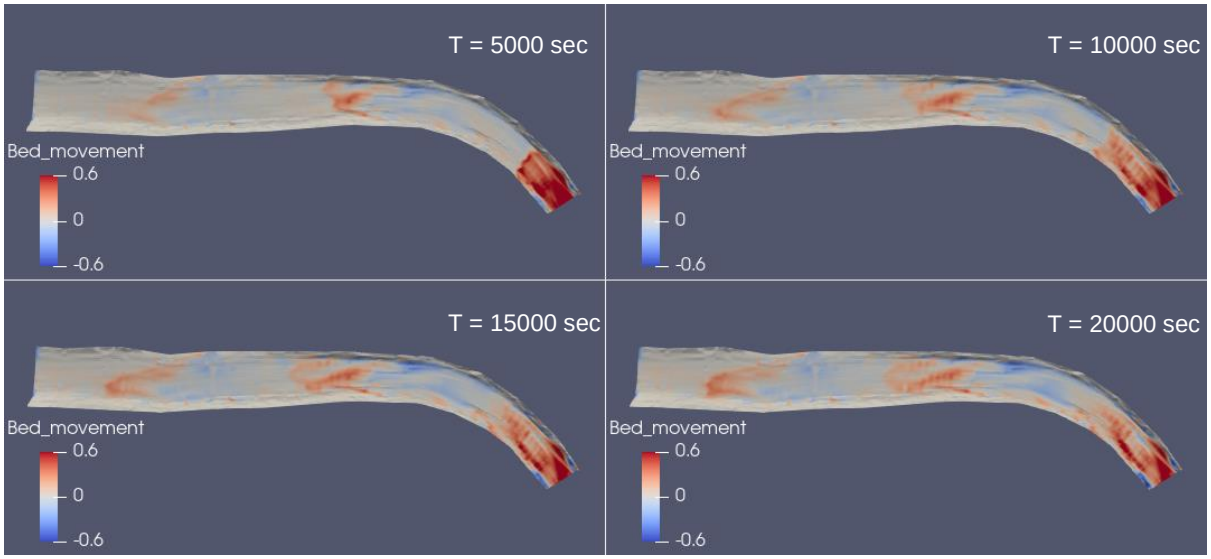

Figure 4.16 Bed movement: Scenario 4 (different timesteps)

In Scenario 4, after 5000 seconds (83 minutes) the majority of the sediment has been introduced into the reach. The sediment is initially deposited in a dune created directly downstream of the inflow boundary (seen in red in the top left quadrant of Figure 4.16) creating a high bed shear stress area with values reaching 140 Pa at the downstream foot of the dune. This in turn starts eroding the bed in this area, moving sediment downstream and shrinking the dune. As the dune shrinks, the shear stress in the area is reduced resulting in a decreasing rate of erosion.

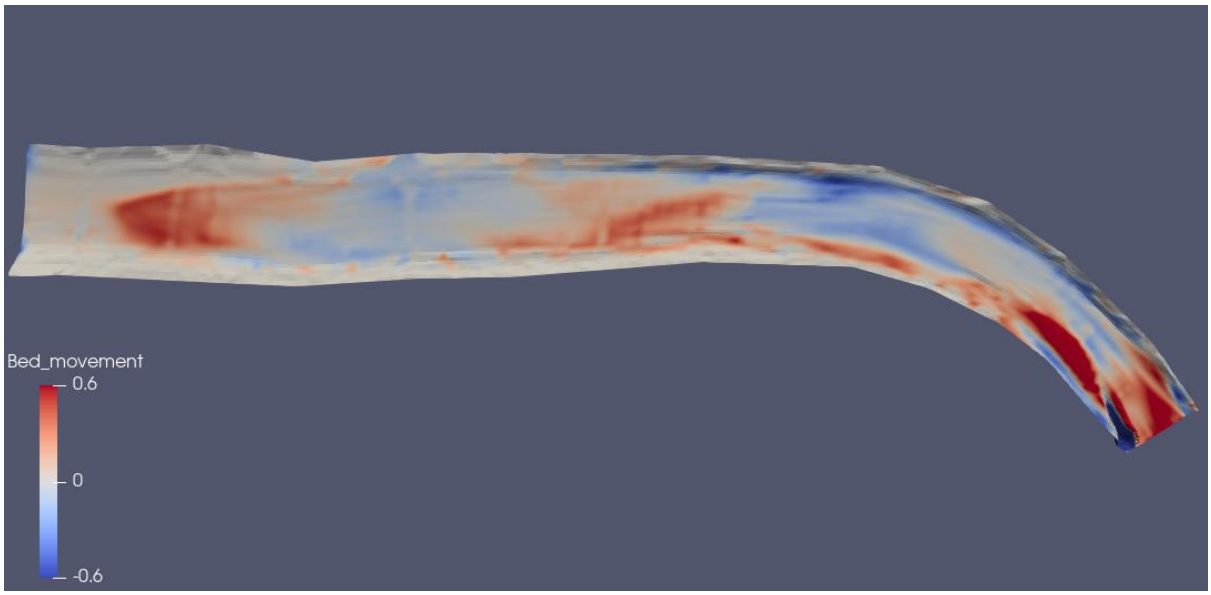

Figure 4.17 Bed movement: Scenario 4

At the end of the simulation, the changes in the bed geometry in Scenario 4 differ from those of the first Scenario (being the control Scenario, having the same initial and boundary conditions without the sediment inflow) in two areas. Some of the sediment introduced is deposited at the inflow, elevating the bed at that area and in addition to that, the deposition area that exists upstream of the outflow boundary is more prominent in this Scenario (Figure 4.17).

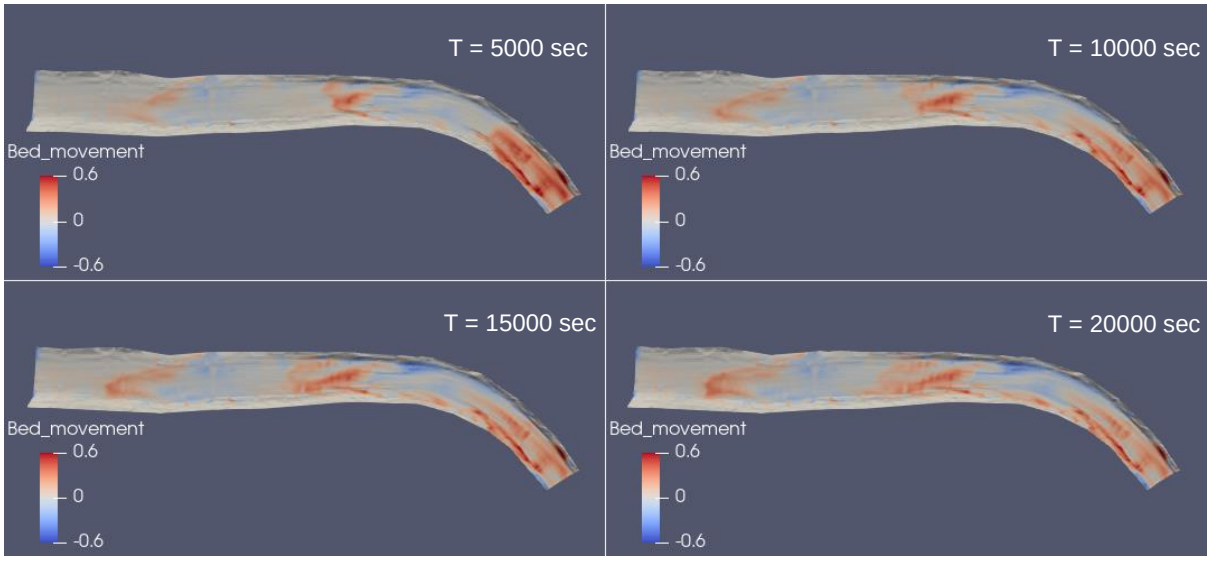

Figure 4.18 Bed movement: Scenario 5 (different timesteps)

In Scenario 5, the composition of the inflowing sediment mixture is finer than that of Scenario 4 making it more erodible. The bed shear stress near the inflow reaches values of 100 Pa in the first 5000 seconds (lower than those of Scenario 4, at 140 Pa) which is enough to immediately transport a lot of the inflowing sediment, creating a less prominent deposition area than that of Scenario 4 (Figure 4.18). The majority of the sediment introduced in the reach in this Scenario is uniformly transported downstream by the flow, with some deposition at the inflow, the shallow water area at the inside of the bend and the main deposition area upstream of the outflow boundary (seen in red in Figure 4.19) and is then flushed away.

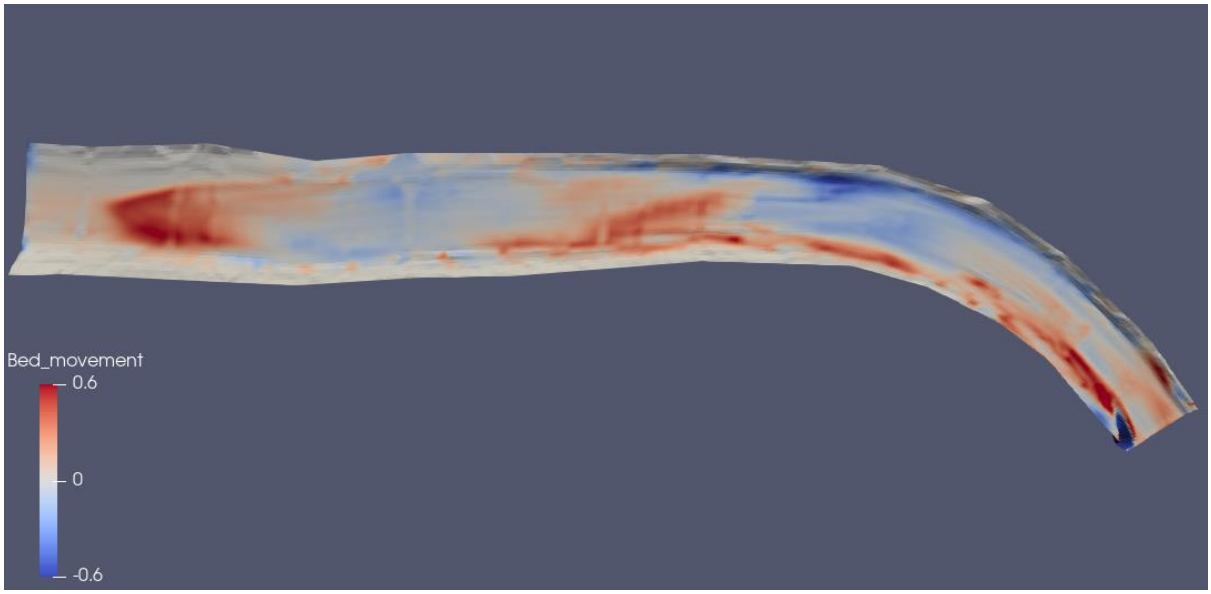

Figure 4.19 Bed movement: Scenario 5

At the end of the simulation, the deposition near the outflow boundary is also more prominent in Scenario 5 (seen in red in Figure 4.19) than in the first Scenario, this area comprises mainly of very fine sediment. Also as seen in Scenario 4, a part of the inflowing sediment is deposited at the inside of the bend where there is a shallow water/low velocity area. At the inflow boundary, small changes are observed compared to the first Scenario, with small sediment deposition areas with heights of 0.25 m as opposed to a uniform erosion of 0.1 m observed in the first Scenario.

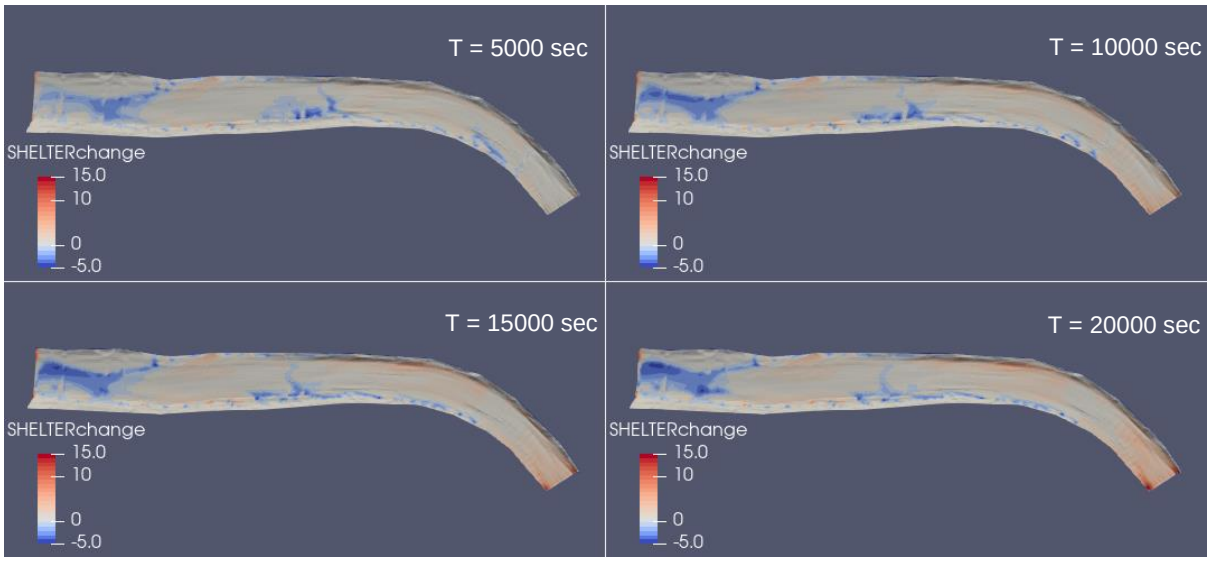

Figure 4.20 Change in number of shelter compared to initial conditions: Scenario 4 (different timesteps)

The change in shelter abundance in the first 20000 seconds (5.5 hours) of Scenario 4 (top left quadrant of Figure 4.20) is identical to that of the first Scenario. Even though a lot of the inflowing sediment is deposited on the bed near the inflow boundary, especially during the first 5000 seconds, (Figure 4.16) it does not significantly affect the bed grain size composition, hence not affecting the D_5 value that is connected to shelter availability.

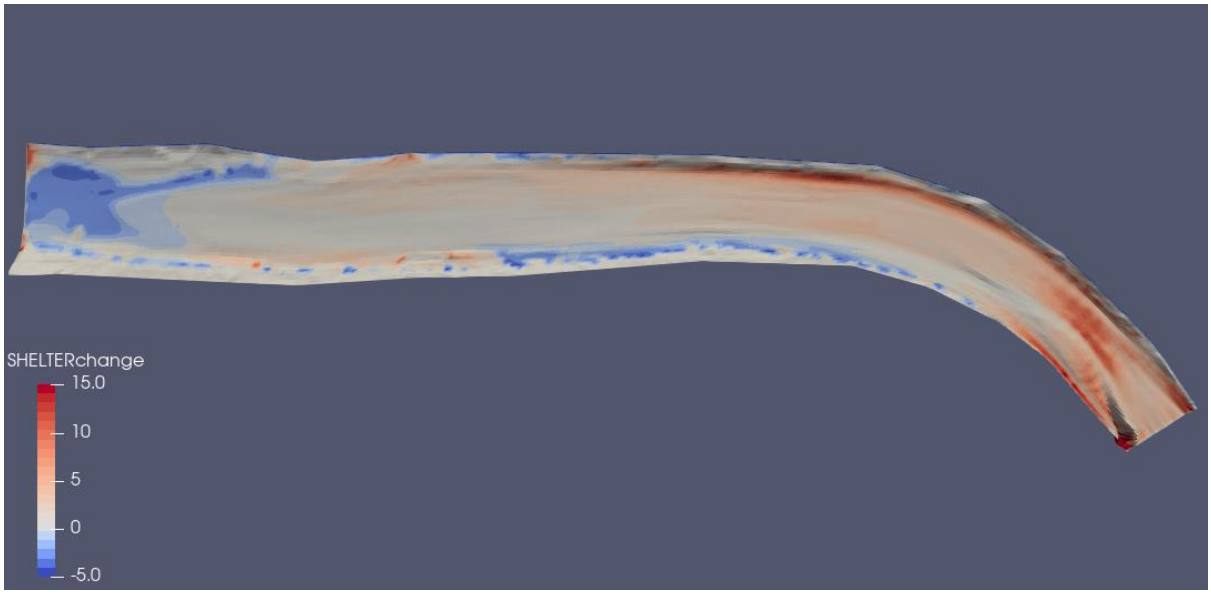

Figure 4.21 Change in number of shelter compared to initial conditions: Scenario 4

Following the pattern of the first 20 timesteps, the resulting changes in shelter availability after 86 timesteps (Figure 4.21), at the end of the simulation are almost identical to those of the first Scenario (Figure 4.6). The area of improved shelter abundance on the outside of the bend is slightly decreased in this Scenario when compared to the first one. Another difference that can be observed between the two Scenarios is an area of increased shelter availability created near the inflow boundary in Scenario 4, this is likely a result of the movement of the sediment eroded from the problematic area on the left-hand side of the inflow boundary and not of the sediment introduced in the first 90 minutes of the simulation, for this reason it is not taken into consideration when interpreting the results.

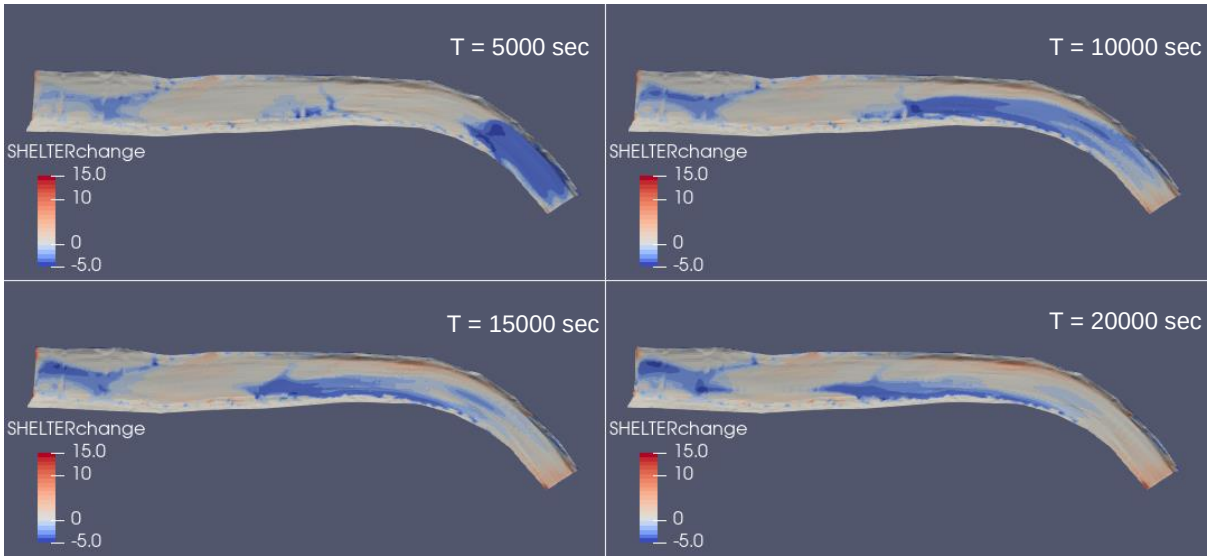

Figure 4.22 Change in number of shelter compared to initial conditions: Scenario 5 (different timesteps)

For Scenario 5, the negative impact the introduced sediment has on the shelter availability of the reach is clear, especially during the first hours of the simulation (Figure 4.22). The inflowing sediment is more spread out than the coarser mixture of Scenario 4, as a result the change in bed geometry is not as noticeable (Figure 4.18) but the fine material significantly reduces the D_5 value of the bed cells. This results in a rolling wave of heavily decreased shelter abundance traveling downstream the reach. After 5000 seconds the fine sediment is concentrated in a distinct area near the inflow boundary (top left quadrant of Figure 4.22). After 10000 seconds the affected area is still distinct but more spread out, travelling downstream. Between 10000 and 15000 seconds, it reaches the shallow water area on the

inside of the bend where it is deposited. After that, the introduced sediment is picked up by the flow and transported downstream to be deposited in the low shear stress area near the outflow or be flushed away from the boundary, reaching an equilibrium after 16 hours.

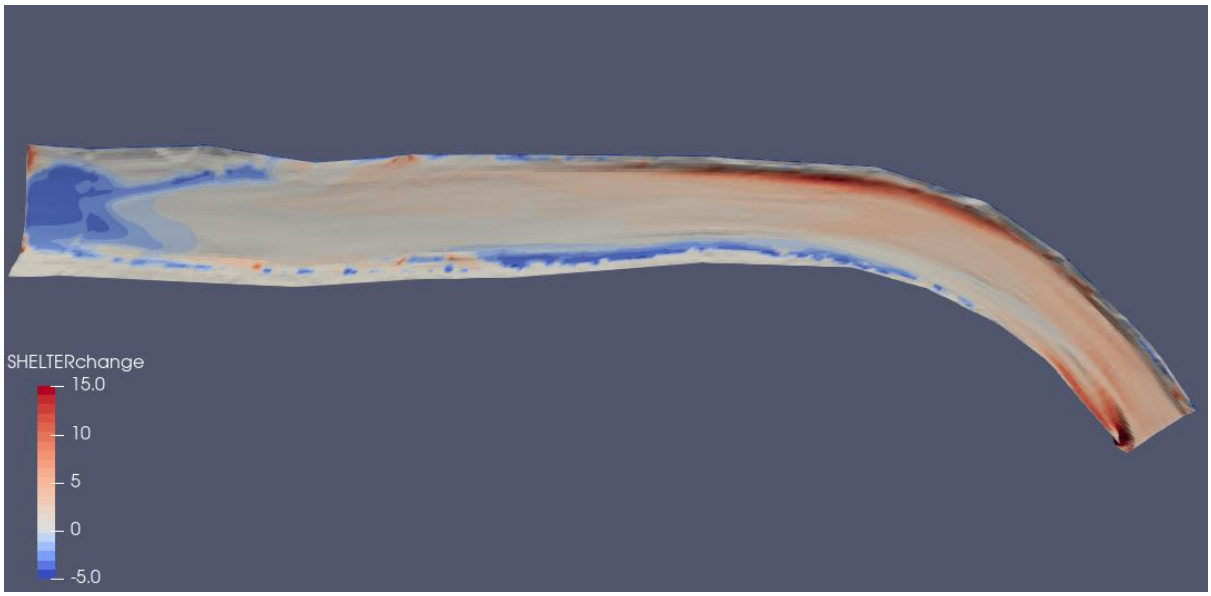

Figure 4.23 Change in number of shelter compared to initial conditions: Scenario 5

At the end of the simulation, the negatively affected area at the inside of the bend has significantly decreased in comparison to the first 20 timesteps (Figure 4.22, Figure 4.23). The resulting shelter availability from Scenario 5 is similar to that of Scenario 1 and 4, the negative impact the inflowing mixture was expected to have is contained in the deposition area near the outflow boundary. In comparison to the other two Scenarios, this area (seen in blue in Figure 4.23) is slightly bigger and the negative impact is stronger, with a big part of the area having 0 shelter availability (very high degree of embeddedness).

5 Conclusion & Discussion

The correlation between the grain size distribution of the river bed (the value of the D_5 percentile in particular), derived by Jocham (2010) by analyzing data measured with the Finstad et al. (2007) method, and the shelter availability for juvenile Atlantic salmon was applied to the results of simulations to predict the habitat conditions in a residual flow channel of a HPP. SSIIM 2, a software comprising of a 3D hydrodynamic model coupled with a morphodynamic model was used to run the simulations. A total of five Scenarios using the same discharge of 100 m^3/s were simulated in the reach of interest.

The substrate composition in Scenarios 1, 4 and 5 is based on the grain size distribution curve derived from field measurements, with Scenarios 4 and 5 having an inflow of two different sediment mixtures for the first 90 minutes of the simulation. Scenarios 2 and 3 assume a very fine sediment composition on the river bed, both of them result in a very erodible bed for the high discharge used in the simulations.

The resulting change in shelter availability in the fine sediment substrate Scenarios was either very limited (Scenario 3) or totally negligible (Scenario 2). This, in conjunction with the high degree of erosion, is interpreted as a sign of uniform sediment transport with respect to the grain size, by picking up and depositing the sediment without segregating fine from coarse grains the flow does not change the D_5 percentile in the cells, hence not changing the shelter availability. The takeaway from these two Scenarios is that if a river bed comprises solely of fine sediment this method predicts small to non-existent changes in shelter availability in a high discharge event like the one simulated.

Scenario 1 serves as a good example for observing changes in shelter availability in a natural river reach, more specifically a regulated residual flow reach where flash flood like events might occur. In this 24-hour simulated event the morphodynamic model predicts changes in the bed geometry in the range of ±60 cm together with significant changes in the spatial distribution of the substrate composition which translate to changes in shelter availability using its dependence on the D_5 value (Figure 4.6).

Another purpose of the results of Scenario 1 is to serve as a baseline against which to compare and interpret the results of Scenarios 4 and 5. These two Scenarios simulate the event of an introduction of a favorable (Scenario 4) and an unfavorable (Scenario 5) sediment mixture for potential shelter availability in the reach. All other parameters of the simulation are identical to those of Scenario 1. In both Scenarios, the majority of the inflowing sediment was flushed away from the outflow boundary during the 24 hours of the simulation. At the end of the simulated period, the impact the favorable mixture had on shelter availability was negligible, while the unfavorable one negatively impacted the shelter availability by exacerbating the reduction of shelter providing crevices in the already negatively affected areas seen in the results of Scenario 1.

Some limitations and problems that should be noted were encountered when setting up the model for this thesis. There was no available depth and velocity data for the discharge used in the simulations, for this reason a very detailed calibration of the model was not possible. Seeing that the purpose of the simulations was to explore the implementation of this method of calculating shelter availability to SSIIM 2 and interpret the results mainly in a comparative way between simulated Scenarios, the lack of measured data to compare them against did not affect the conclusions. Some computational difficulties were encountered in a specific area at the inflow boundary of all simulations, causing a very small area of high bed shear stress and high erosion, the effect this had on the results was very limited and not taken into consideration when interpreting them.

Both the accuracy with which the impact of inflowing sediment on shelter availability was captured and the final results are promising, indicating that using the Finstad et al. (2007) method and the correlation Jocham (2010) derived in conjunction with a numerical model can give useful insight into the processes undertaken and make predictions for potential shelter availability. Further implementation of this method should be investigated in SSIIM 2, as it already has a more holistic approach to river modeling in comparison to simpler hydrodynamic modeling software by coupling the hydrodynamic processes to a morphodynamic model. This method could also be combined with other methods of shelter abundance and substrate condition calculation used in habitat modeling software.

6 Publication bibliography

Armstrong, J.D; Grant, James W.A.; Forsgren, Harvey L.; Fausch, Kurt D.; DeGraaf, Richard M.; Fleming, Ian A. et al. (1998): The application of science to the management of Atlantic salmon (Salmo salar): integration across scales.

Armstrong, J.D; Kemp, P.S; Kennedy, G.J.A; Ladle, M.; Milner, N.J (2003): Habitat requirements of Atlantic salmon and brown trout in rivers and streams. In *Fisheries Research* 62 (2), pp. 143–170. DOI: 10.1016/S0165-7836(02)00160-1.

Boussinesq, J. (1877): Essai sur la theorie des eaux courantes. Memoires presentes par divers savants a l'Academie des Sciences.

Bunte, Kristin; Abt, Steven R. (2001): Sampling surface and subsurface particle-size distributions in wadable gravel-and cobble-bed streams for analyses in sediment transport, hydraulics, and streambed monitoring.

Eastman, K. (2004): Effects of Embeddedness on Fish Habitats: An Approach for Implementation in the Habitat Simulation Model CASiMiR. University of Stuttgart.

Esteve, Manu (2005): Observations of Spawning Behaviour in Salmoninae: Salmo, Oncorhynchus and Salvelinus. In *Rev Fish Biol Fisheries* 15 (1-2), pp. 1–21. DOI: 10.1007/s11160-005-7434-7.

Eurostat (2020): Renewable energy in the EUin 2018. Available online at https://ec.europa.eu/eurostat/documents/2995521/10335438/8-23012020-AP-EN.pdf/292cf2e5-8870-4525-7ad7-188864ba0c29, updated on 2020, checked on 1/10/2021.

Finstad, A. G.; Einum, S.; Forseth, T.; Ugedal, O. (2007): Shelter availability affects behaviour, size-dependent and mean growth of juvenile Atlantic salmon. In *Freshwater Biol* 52 (9), pp. 1710–1718. DOI: 10.1111/j.1365-2427.2007.01799.x.

Fitzpatrick, Faith A.; Waite, Ian R.; D'Arconte, Patricia J.; Meador, MIchael R.; Maupin, Molly A.; Gurtz, Martin E. (1998): Revised Methods for Characterizing Stream Habitat in the National Water-Quality Assessment Program.

Forseth, Torbjørn; Harby, Atle (Eds.) (2014): Handbook for environmental design in regulated salmon rivers. CEDREN.

Fraser, Neil H. C.; Metcalfe, Niel B.; Thorpe, John E. (1993): Temperature-Dependent Switch between Diurnal and Nocturnal Foraging in Salmon.

Hedger, R. D.; Dodson, J. J.; Bergeron, N. E.; Caron, F. (2005): Habitat selection by juvenile Atlantic salmon: the interaction between physical habitat and abundance. In *J Fish Biology*.

Heggenes, J.; Baglinière, J. L.; Cunjak, R. A. (1999): Spatial niche variability for young Atlantic salmon (Salmo salar) and brown trout (S. trutta) in heterogeneous streams. In *Ecology of Freshwater Fish*.

Heggenes, Jan (1990): Habitat utilization and preferences in juvenile atlantic salmon (salmo salar) in streams. In *Regul. Rivers: Res. Mgmt.* 5 (4), pp. 341–354. DOI: 10.1002/rrr.3450050406.

International Renewable Energy Agency (2020). Available online at https://www.irena.org/europe, updated on 2020, checked on 1/10/2021.

Jocham, Stefan (2010): An approach to link shelter abundance and grain size distribution for the assessment of sediment quality for juvenile Atlantic salmon.

Kondolf, G. Mathias; Piégay, Hervé (2003): Tools in fluvial geomorphology. Chichester: J. Wiley.

Kondolf, G. Mathias; Wolman, M. Gordon (1993): The sizes of salmonid spawning gravels. In *Water Resour. Res.* 29 (7), pp. 2275–2285. DOI: 10.1029/93WR00402.

Launder, B. E.; Spalding, D. B. (1974): The numerical computation of turbulent flows. In *Computer Methods in Applied Mechanics and Engineering* 3 (2), pp. 269–289. DOI: 10.1016/0045-7825(74)90029-2.

Mills, Derek Henry (1989): Ecology and management of Atlantic Salmon.

Morantz, D. L.; Sweeney, R. K.; Shrivell, C. S.; Longard, D. A. (1987): Selection of Microhabitat in Summer by Juvenile Atlantic Salmon (Salmo salar). In *Canadian Journal of Fisheries and Aquatic Sciences* 44.

Olsen, Nils Reidar B. (2018): A three-dimentional numerical model for simulation of sediment movements in water intakes with multiblock option. SSIIM User's Manual. NTUA.

Portuguese Renewable Energy Association (2020). Available online at https://www.apren.pt/en/renewable-energies/highlights/, updated on 2020, checked on 1/10/2021.

Rimmer, D. M.; Paim, U.; Saunders, R. L. (1984): Changes in the Selection of Microhabitat by Juvenile Atlantic Salmon (Salmo salar) at the Summer–Autumn Transition in a Small River. In *Can. J. Fish. Aquat. Sci.* 41 (3), pp. 469–475. DOI: 10.1139/f84-056.

Scheurer, Karin; Alewell, Christine; Bänninger, Dominik; Burkhardt-Holm, Patricia (2009): Climate and land-use changes affecting river sediment and brown trout in alpine countries--a review. In *Environmental science and pollution research international* 16 (2), pp. 232–242. DOI: 10.1007/s11356-008-0075-3.

Schwarzwalder, Kordula; Rüther, Nils; Alfredsen, Knut; Albayrak, Ismail (2018): Various Sediment Measurement Methods and Techniques as Basis for Habitat Quality Evaluation in the River Section of HPP Schiffmühle. DOI: 10.3929/ETHZ-B-000308182.

Shields, A. (1936): Application of similarity principles and turbulence research to bed load movement.

Shirvell, C. S.; Dungey, R. G. (1983): Microhabitats Chosen by Brown Trout for Feeding and Spawning in Rivers. In *Transactions of the American Fisheries Society* 112 (3), pp. 355–367. DOI: 10.1577/1548-8659(1983)112%3C355:MCBBTF%3E2.0.CO;2.

Sylte, Traci; Fischenich (2003): An Evaluation of Techniques for Measuring Substrate Embeddedness.

Symons, P. E. K.; Heland, M. (1978): Stream Habitats and Behavioral Interactions of Underyearling and Yearling Atlantic Salmon (Salmo salar). In *J. Fish. Res. Bd. Can.* 35 (2), pp. 175–183. DOI: 10.1139/f78-029.

Szabo-Meszaros, Marcell (2015): Shelter for juvenile Atlantic salmon: availability and prediction in rivers with and without hydropower regulation.

Valdimarsson, S. K.; Metcalfe, N. B. (1998): Shelter selection in juvenile Atlantic salmon, or why do salmon seek shelter in winter? In *J Fish Biology*.

van Rijn, Leo C. (1984): Sediment Transport, Part I: Bed Load Transport. In *Journal of Hydraulic Engineering* 110.

Winston, Wayne L. (2004): Operations Research. 3rd: Wadsworth Publishing Co.

7 Appendices

APPENDIX A

Sieving results

FIThydro NTNU

Sample site	Schiffmühle / Limmat
Date of survey	13-15.03.2018
Sample number	Curve 1, aggregate
Date of sieving	5/4/2018
mass analysis dry [g]	214255.5

sieve [mm]	residue [g]
170	4428.0
120	16553.2
100	25567.7
80	30232.7
60	38619.7
40	51174.1
20	35097.6
16	4986.3
14	1827.1
12.5	1351.2
10	1704.4
8	1010.0
6	683.3
4	507.0
2	246.3
1	95.2
0.5	52.3
<0,5	119.4

Sieving results
(artificial)

Sample site	Schiffmühle / Limmat	Schiffmühle / Limmat
Sample number	Curve 2	Curve 3
mass analysis dry [g]	14217.1	19217.1

sieve [mm]	**residue [g]**	**residue [g]**
170	6.1	506.1
120	0.9	500.9
100	2.4	502.4
80	34.5	534.5
60	175.6	675.6
40	306.1	806.1
20	479.1	979.1
16	786.9	1286.9
14	568.0	1068.0
12.5	732.0	1232.0
10	1395.6	1395.6
8	5688.0	5688.0
6	3615.0	3615.0
4	426.9	426.9
2	0.0	0.0
1	0.0	0.0
0.5	0.0	0.0
<0,5	0.0	0.0

APPENDIX B

```
clc

clear

filesfracres= dir('*.new');

filesvtk= dir('*.vtk');

filename= 'original.txt';

fileid= fopen(filename);

B= textscan(fileid, '%f');

fclose(fileid);

originalarray= B{1, 1};

d5original= 15.2501;

shelteroriginal= 0.39*d5original + 0.37;

sieve= [0.5, 1, 2, 4, 6, 8, 10, 12.5, 14, 16, 20, 40, 60, 80, 100, 120, 170];

for iouter= 1:87

        fileid= fopen(filesfracres(iouter).name);

        A= textscan(fileid, '%f');

        fclose(fileid);

        array= A{1, 1};

        cellcounter= 1;

        d5counter= 1;

        k= 1;

        k5=1;

        ch= 1;

        iter= length(array);

        reversing= length(array)+ 1;

        for i= 1:length(originalarray)

                aggregate(i)=0;

        end

        for i= 1:iter

                if  ((k5== 37) || (k5== 38))
```

```
                        d5array(d5counter, (39- k5))= array(reversing- i);

                        if (k5== 38)

                                flagd5= 0;

                                for ii= 1:length(originalarray)

                                        if  aggregate(ii)>= 0.05 && flagd5 == 0

                                        btw(1)= ii;

                                        flagd5= 1;

                                end

                                if  aggregate(ii)>= 0.5

                                        btw(2)= ii;

                                        break

                                end

                        end

                                d5array(d5counter, 3)= (sieve(btw(1)- 1))+ ((sieve(btw(1))-
                sieve(btw(1)- 1))/(aggregate(btw(1))- aggregate(btw(1)- 1))*(0.05-
                aggregate(btw(1)- 1)));

                                d5array(d5counter, 4)= (sieve(btw(2)- 1))+ ((sieve(btw(2))-
                sieve(btw(2)- 1))/(aggregate(btw(2))- aggregate(btw(2)- 1))*(0.5-
                aggregate(btw(2)- 1)));

                                k5= 0;

                        d5counter= d5counter+ 1;

                end

                elseif ((k5== 18) || (k5== 36))

                elseif (k5== 19)

                        aggregate(k5- 18)= array(reversing- i);

                elseif  ((k5>= 20) && (k5<= 35))

                        aggregate(k5- 18)= array(reversing- i)+ aggregate(k5- 19);

                else

                end

                k5= k5+ 1;

        end

        sheltermap= zeros(298, 40);

        for i= 2:298
```

```
        for j= 2:40
                sheltermap(i, j)= 0.39*d5array(length(d5array)+ 2- j- 39*(i-2), 3) + 0.37;
        end
end
d50map= zeros(298, 40);
for i= 2:298
        for j= 2:40
                d50map(i, j)= d5array(length(d5array)+ 2- j- 39*(i-2), 4);
        end
end
zz= 0;
fileid= fopen(filesvtk(iouter+87).name, 'a');
fprintf(fileid, '\n \nSCALARS SHELTER float\nLOOKUP_TABLE default\n');
fprintf(fileid, '\n');
for i= 1:40
        for j= 1:298
                fprintf(fileid, '%f ', sheltermap(j, i));
        end
        fprintf(fileid, '%f ', zz);
        fprintf(fileid, '\n');
end
for i= 1:299
        fprintf(fileid, '%f ', zz);
end
fprintf(fileid, '\n \nSCALARS SHELTERchange float\nLOOKUP_TABLE default\n');
fprintf(fileid, '\n');
for i= 1:40
        for j= 1:298
                fprintf(fileid, '%f ', sheltermap(j, i)- shelteroriginal);
        end
```

```
        fprintf(fileid, '%f ', zz);
        fprintf(fileid, '\n');
end
for i= 1:299
        fprintf(fileid, '%f ', zz);
end
fprintf(fileid, '\n \nSCALARS D50 float\nLOOKUP_TABLE default\n');
fprintf(fileid, '\n');
for i= 1:40
        for j= 1:298
                fprintf(fileid, '%f ', d50map(j, i));
        end
        fprintf(fileid, '%f ', zz);
        fprintf(fileid, '\n');
end
for i= 1:299
        fprintf(fileid, '%f ', zz);
end
fclose(fileid);
end
```